Sex-Specific Development of ssRNA Virus Receptor Gene Expression in the Human Brain

Negeen Halabian[1*] Leanne Monteiro[1*] Lisa Jiawei[2] Maheshwar Panday[1] Kathryn M. Murphy[1,2]

[1] McMaster Neuroscience Graduate Program, McMaster University, Hamilton, ON, L8S 4K1, Canada
[2] Department of Psychology, Neuroscience & Behavior, McMaster University, Hamilton, ON, L8S 4K1, Canada
* These authors contributed equally to this project

Correspondence should be addressed to Kathryn M. Murphy; kmurphy@mcmaster.ca
Kathryn Murphy, Department of Psychology, Neuroscience & Behavior, McMaster University, McMaster University, 1280 Main Street West, Hamilton, ON L8S 4K1, Canada.

Article Type: ***Technology and Code Article***: Abstract 299 words; Tables/Figures 0/15; Manuscript 9181 words; Supplementary Material 3 tables, 3 figures and R Markdowns.

Authors' contributions: NH designed research, performed research, analyzed data, wrote/revised the paper; LM performed research, analyzed data, wrote/revised the paper; LJ performed research, analyzed data; MP analyzed data, wrote/revised the paper; KM designed research, analyzed data, wrote/revised the paper.

Acknowledgements: We recognize that our McMaster University laboratory is located on the traditional territories of the Mississauga and Haudenosaunee nations and within the lands protected by the "Dish with One Spoon" wampum agreement. We thank Rachel Kwan, Brendan Kumagai, Ewalina Jeyanesan, Luke Bai and Adam Gee for help with coding. The transcriptomic data were from (Kang et al., 2011) (GSE25219).

Funding Sources: NSERC Grant RGPIN-2020-06403 awarded to KM, NSERC CGS-M awarded to LM and NH, OGS awarded to MP. The funder had no role in study design, data collection and analysis, decision to publish, or manuscript preparation.
Data and Code Availability: The data used to support the findings in this manuscript and code are available here: https://osf.io/wjthz/

Conflict of Interest Statement: The authors declare that the research was conducted in the absence of any commercial or financial relationships that could be construed as a potential conflict of interest.

Abstract

Viral infection severity often varies with host factors such as age and sex. The pathogenesis of infections caused by a broad range of viruses, from neurotropic viruses like Rabies and Zika to respiratory viruses such as influenza and SARS-CoV-2, differ between the sexes and across the lifespan. Typically, older males are more susceptible to severe acute outcomes, while females are more vulnerable to the post-acute sequelae of infections. All of these complications can include neuroinflammation, stroke, cognitive dysfunction, and delirium. While these symptoms can be secondary to infection, recent studies suggest that even peripheral infections can lead to neuropathological changes in the brain. However, few studies have characterized the expression of viral receptors in the human brain or examined age- or sex-related differences in such expression. In this study, we used a publicly accessible transcriptomic database to assess the impact of age and sex on the expression of 67 viral host factor genes, associated with ten virus families. Analyzing data from 15 brain areas (n=33, F=14, M=19, age:4 mo-80 yrs), we determined the lifespan trajectory for each gene in each area via LOESS regressions. We used unsupervised hierarchical clustering to determine if a brain-wide pattern or virus family pattern can be detected. Using Dense-tSNE, a dimension-reduction and visualization technique, we discovered four distinct developmental trajectories, clustering the areas into two mixed-sex subcortical clusters and one each of male and female cortical clusters. Applying Differential Expression Sliding Window Analysis (DeSWAN), we identified the genes driving these age- and sex-related differences. Many sex differences were noted in childhood, potentially impacting the brain's susceptibility to viral infections and underscoring a broader dimorphic organization of male and female brains. These insights contribute to our understanding of sex-specific responses to viral infections, offering the potential for more personalized treatment strategies.

Introduction

The recent COVID-19 pandemic, Zika virus outbreak and surge in Dengue fever highlight the escalating threat to public health of neuroinfectious diseases transmitted by single-strand RNA (ssRNA) viruses (Bohmwald et al., 2018a; Morgello, 2020a; Sun et al., 2020). The intensity, persistence, and fatality of neurological symptoms triggered by viral diseases vary markedly among individuals (Morgello, 2020b; Paniz‑Mondolfi et al., 2020; Wehbe et al., 2021; Wouk et al., 2021a; Levine et al., 2023) and are influenced by host factors such as age and sex (Mauvais-Jarvis et al., 2020; Takahashi et al., 2020a; Zhou et al., 2020; Sudre et al., 2021). However, little is known about the expression of virus receptors in the human brain, especially how receptor levels vary by age and sex across cortical and subcortical structures. Viral pathogens can trigger acute and post-acute neurological symptoms, from mild reversible symptoms such as headache, fever, anosmia, ageusia, confusion and memory problems to more severe symptoms such as encephalitis, meningitis, stroke, paralysis and even death (Koyuncu et al., 2013; Cheng et al., 2020; Engin et al., 2021). Understanding age- and sex-related patterns of virus receptor expression in the human brain may provide new insights into the neurological consequences of certain viral diseases. Here we use transcriptomic data on ssRNA viral receptor expression in the human brain to characterize and compare the development of those markers in females and males.

Various host factors, such as environment, virus characteristics, and host conditions, influence viral infections' intensity, prevalence, and pathogenesis. A growing body of evidence emphasizes the importance of sex and age as dominant factors impacting how humans respond to viral infection (Peretz et al., 2015; Mauvais-Jarvis et al., 2020; Jacobsen and Klein, 2021; Samadizadeh et al., 2021). For example, men and older COVID-19 patients were more likely to

be admitted to hospital, require ICU care and have a greater risk of death (Kaeuffer et al., 2020; Prado-Galbarro et al., 2020; Rosenthal et al., 2020; Scully et al., 2020; Gujski et al., 2021; Murthy et al., 2021; Rao et al., 2021). Similarly, other Coronaviridae, such as SARS and MERS, showed a male bias in morbidity and mortality (Kumar et al., 2021; Wouk et al., 2021b). In contrast, post-acute-sequelae of COVID-19, commonly known as Long Covid, is more severe and persistent in women than men (Sudre et al., 2021). Furthermore, women are more susceptible to certain viral infections, such as the Influenza A virus, with higher morbidity and mortality than men (Aaby et al., 1986; Klein and Huber, 2009; Klein et al., 2012; Morgan and Klein, 2019; Giurgea et al., 2021).

Viral particles can enter the brain via direct or indirect routes, and while the immune response rapidly clears most viruses, some can persist (Nath and Johnson, 2022). Even cleared viruses may have already infected cells in the brain, leaving behind a range of neurological changes. For example, a recent study showed that SARS-CoV-2 infection can induce neurons and glia to fuse with neighbouring cells and create multinucleated syncytia, allowing for viral propagation from within one cell to the next (Martínez-Mármol et al., 2023a). That process depends on receptors and co-factors such as hACE2, TMPRSS2 and NRP1 (Martínez-Mármol et al., 2023a). Moreover, other viruses such as rabies virus, Japanese encephalitis virus, vesicular stomatitis virus, poliovirus, measles virus, herpes simplex virus, varicella-zoster virus, Zika virus, dengue virus, Nipah virus, chikungunya virus can cause syncytia to form in pulmonary and cardiac tissue (Martínez-Mármol et al., 2023b). Viral infections may also lead to transcriptomic and structural changes in the host cells, such as the molecular signatures of brain aging and loss of cortical gray matter observed after severe COVID-19 infections (Douaud et al., 2022; Mavrikaki et al., 2022; Zhang et al., 2022). These findings highlight the potential for viruses to

trigger pathological changes in the brain that cause multiple neurological abnormalities (Mishra and Banerjea, 2020).

More than half of all virus-host interactions in mammals involve ssRNA viruses, many of which have known sex disparities in their impact (Klein et al., 2012; Klein and Flanagan, 2016; Scully et al., 2020). In this study, we used transcriptomic data of ssRNA virus receptor expression and a unique lifespan trajectory analysis to characterize sex- and age-related changes in virus receptors in the human brain. We found a surprising number of sex differences in the lifespan trajectories of ssRNA virus receptors in the human brain.

Methods

Human Tissue Samples and Datasets

The Hamilton Integrated Research Ethics Board approved the study. The postnatal human brain's spatiotemporal development of viral receptor genes was characterized using transcriptomic data collected by Kang et al. (2011) (GSE25219). For the current study, only data from the postnatal cases were used that included 52 cases (23 females, 29 males) ranging in age from 4 months to 82 years. A detailed description of tissue acquisition and processing, data generation, validation and analyses can be found in the Supplementary Material from Kang et al. (2011). Notably, the original study ran quality tests on the samples (PMI, pH, RIN, and DS) to validate their suitable for transcriptomic profiling, and factors such as postmortem interval (PMI) did not positively correlate with expression levels. Here, we provide a brief overview of the tissue processing that produced this valuable dataset.

The publicly available dataset used in this study was selected because it has a wide range of ages making it the most comprehensive transcriptomic dataset of lifespan changes in the human brain. Kang et al. (2011) obtained the postmortem human brain samples from the Yale University School of Medicine, the Clinical Brain Disorders Branch of the National Institute of Mental Health, the Human Fetal Tissue Repository at the Albert Einstein College of Medicine (AECOM), the Brain and Tissue Bank for Developmental Disorders at the University of Maryland, the Birth Defects Research Laboratory at the University of Washington, Advanced Bioscience Resources Inc. and the MRC-Wellcome Trust Human Developmental Biology Resource at the Institute of Human Genetics, University of Newcastle, UK. The brain areas of interest were matched between specimens, ages, and brain hemispheres. Fresh tissue samples

were obtained from the Yale University School of Medicine and the Human Fetal Tissue Repository at AECOM cases. The other samples were obtained from frozen tissue specimens stored at -80 ºC. For the current study, data from 15 brain areas were analyzed, including 11 cortical and 4 subcortical brain areas (Supplementary Material Table 1).

Tissue Sample Processing

Briefly, tissue samples were lysed, RNA was extracted (RNeasy Plus Mini Kit, Qiagen), followed by DNase treatment (TURBO DNase, Ambion). The RNA integrity number (RIN) was determined for each sample using Bioanalyzer RNA 6000 Nano Kit or Bioanalyzer RNA 6000 Pico Kit (Agilent) (RIN 8.83 ± 0.93 (mean ± s.d.)). The total RNA extracted underwent reverse transcription (RT) to generate cDNA. The Affymetrix Human Exon Microarray was used to measure gene expression levels for 17,565 probes. The raw exon array data were normalized using the Partek Genomics Suite (version 6.5, default Partek settings) and RNA background correction, quantile normalization, mean probe set summarization, and log2-transformation were performed.

Data Analysis Pipeline

Data Preparation and Brain Areas Studied: We retrieved the transcriptomic data generated by Kang et al. (2011) from the Gene Expression Omnibus (GSE25219) and prepared it into a working file for the current study (see Supplementary Material for a detailed description of the steps)(https://osf.io/4fgka). The prepared data file included information for 17,528 genes and metadata for each case (e.g. age, sex, brain area, PMI, cause of death etc.). The original dataset had been log2 transformed and included transcriptomic data from 27 brain areas. However, 12 areas did not have enough cases to construct lifespan trajectories for both females and males, so

15 areas were used for this study (see Supplementary Material). Of the 15 brain areas, 5 were from the frontal cortex (OFC, DFC, VFC, MFC, M1C), 2 parietal cortex (S1C, IPC), 3 temporal cortex (A1C, STC, ITC), 1 occipital cortex (V1C), 1 hippocampus (HIP), 1 amygdala (AMY), the medial dorsolateral nucleus of the thalamus (MD), and the cerebellum (CBC). Supplementary Material Table 1 includes information about which cases had data from the various brain areas.

Viral Receptors Studied: We studied 67 human virus receptors and SARS-CoV-2 host factors responsible for mediating the entry of ssRNA viruses into cells. The receptor genes were selected from a curated database (http://www.computationalbiology.cn:5000/viralReceptor/type?type=4) (Zhang et al., 2019). Those receptors mediate cell entry for 10 different virus families, and the genes responsible for those receptors were identified in the transcriptomic dataset. Supplementary Material Table 2 lists the gene symbols, names of the virus receptors, virus species and virus families.

Visualization of Lifespan Trajectories for the Virus Receptor Genes: We calculated the lifespan trajectories by z-scoring the expression for each gene and all 15 brain areas. That step ensured that the trajectories represent change across the lifespan rather than the amount of gene expression. Next, locally estimated scatterplot smoothing (LOESS) curves with 128 points were fit separately to the female and male z-scored data using the LOESS function in base R (span value of 0.75 and 95% confidence intervals (CI)). The curves were plotted with age on a log scale to better represent and visualize the rate of change that occurs across the lifespan, with rapid development in infancy and childhood and slower changes through adulthood (Supplementary Fig. 1). These steps produced 2010 trajectories (2 sexes X 15 brain areas X 67 virus receptors).

Clustering Virus Receptor Genes Trajectories: The dimensionality of the data was reduced by performing unsupervised hierarchical clustering of the LOESS trajectories using the Ward.d2 algorithm (hclust function in base R). The resulting trajectory clusters reflect the minimum number of trajectories that captured how virus receptor gene expression changed across the lifespan in female and male brains. First, all 2010 trajectories were clustered to examine the overall range of trajectories and assess for sex biases in the trajectories where one sex was more likely to have virus receptor genes that followed a particular pattern. Second, the trajectories for genes in each of the 10 virus families were clustered separately. Third, the trajectories within the 15 brain areas were clustered independently. For each analysis, we selected the number of clusters (k) by calculating the total within-cluster sums of squares (WCSS) for a range of k and applying the elbow method ("elbow" package in R) and generating the average trajectory for each cluster. Finally, we validated the uniqueness of the cluster trajectories using the Fréchet distance metric to compare the shapes of the trajectories while maintaining the orderly progression of age (Alt and Godau, 1995). The Fréchet distance is 0 for identical trajectories, and the greater the difference between the trajectories, the larger the Fréchet distance. All pairwise comparisons between the cluster trajectories were made, and the resulting Fréchet distances were analyzed using Estimation statistics (Ho et al., 2019). In all cases, the distribution of Fréchet distances showed similarity within clusters and different trajectories between clusters, thereby validating the unique patterns of molecular brain development identified by the different clusters.

To quantify sex differences, we started by calculating a Sex Bias index (SBI) for each cluster, which could range from +1 if a cluster had only female trajectories to 0 for an equal

number of female and male trajectories to -1 for only male trajectories. The SBI was calculated for each cluster using the following equation:

Equation 1:

$$SBI = \frac{(n\ of\ Female\ Trajectories - n\ of\ Male\ Trajectories)}{(n\ of\ Female\ Trajectories + n\ of\ Male\ Trajectories)}$$

In addition, clusters were labelled based on the ratio of female to male trajectories within the cluster. For example, a cluster labelled F100:M0 had only female trajectories.

Analysis of Sex Differences within Virus Families and Brain Areas: In addition to the SBI calculated for individual clusters, an overall sex Dimorphism Score (DS) was calculated for each virus family and brain area. The DS provided information on the overall strength of the sex differences across the clusters and could vary from +1, where all clusters contained trajectories from only one sex to 0, where all clusters had an equal number of female and male trajectories.

Equation 2:

$$DS = |SBI\ cluster\ 1| + |SBI\ cluster\ 2| + \ldots\ /\ number\ of\ clusters$$

Visualizing High-Dimensional Developmental Trajectories in 15 Brain Areas: The Sex-specific development of each brain area was characterized by visualizing the high-dimensional trajectory created by the 67 virus receptor genes separately for females and males. t-SNE (t-Distributed Stochastic Neighbor Embedding) (Maaten and Hinton, 2008) was used to map the high-dimensional data onto 2 dimensions (2D). Here we applied a recent extension of t-SNE, dense t-SNE, because it preserves local and global structure in the data when projecting it onto 2D. For each brain area, the 67 virus receptor gene trajectories for each sex were used as the input to the den-SNE (Narayan et al., 2021) function from the densVIS package in R. We examined a range of perplexity values, and 30 was selected as the best representation of

the data structure (dens_lambda= 0.1 and dens_frac= 0.9). The points in the plot were colour-coded based on sex or age.

Differential Expression-Sliding Window ANalysis (DE-SWAN): To identify virus receptor genes with different expression levels between females and males across the lifespan, we applied Differential Expression-Sliding Window ANalysis (DE-SWAN) (Lehallier et al., 2019). DE-SWAN allowed for the detection of genes with significantly different expression levels in females and males at a series of overlapping ages across the lifespan. The analysis window was stepped across the LOESS curves of lifespan changes to identify the number of differentially expressed genes. The robustness of the DE-SWAN results was assessed by plotting the analysis for a range of p-values ($p=0.001$, $p=0.01$, $p=0.05$) and window sizes (4 yrs, 20 yrs, 40 yrs). Ages with a consistently higher or lower number of differentially expressed genes across the p-values were selected as the reference ages. Statistical comparisons between the expression of the 67 virus receptor genes in females and males were made at each reference age. The Benjamini-Hochberg procedure was used to correct for multiple comparisons, and the q-value was calculated for each gene to control the false discovery rate (FDR) and identify genes with significant differential expression (q-value<0.05). The results were visualized in a heatmap with 67 rows for the genes and 13 columns for the reference ages. The cells in the heatmap were colour-coded pink when females expressed more of the gene and green when males expressed more. The order of the rows was determined by a surrounding dendrogram so that genes with similar patterns of sex differences across the lifespan were grouped.

Results

Non-linear undulating development of viral receptors in female and male brains

We applied a data-driven approach to characterize the development of virus receptors in the human brain and assess sex differences. LOESS curves were fit separately to the female and male data to create lifespan 2010 trajectories for the 67 genes in each of the 15 brain areas (2 sexes X 67 virus genes X 15 brain areas). We called each of those curves a *gene/brain area trajectory* and used that term to describe the results generated from the data for the expression of one virus gene in one brain area and from one sex.

Figure 2 shows the gene/brain area trajectories for the virus receptor ACE2. The ACE2 trajectories illustrate the range of patterns found for the virus receptors where most followed a non-linear undulating pattern of change across the lifespan. Further inspection of the other virus receptors showed a similar range of trajectory shapes (Supplementary Material Fig. 1). Notably, many of the pairs of female and male trajectories followed different patterns, often changing in opposite directions at particular ages (e.g. ACE2 in the VFC, OFC, STC brain areas).

Unsupervised clustering of the 2010 trajectories identified 25 clusters; the smallest cluster had 19 trajectories, while the largest cluster had 153 trajectories (Fig. 3A). Details about the virus receptor genes, brain areas and sex of the trajectories in each cluster are listed in Supplementary Material Table 3. We compared the shape of the cluster trajectories using Frechet distance metric analysis (Alt and Godau, 1995) and Estimation statistics (Calin-Jageman and Cumming, 2019) and found strong between-cluster differences, supporting the conclusion that the clusters represented 25 unique trajectories of virus receptor gene development in the human brain.

Each trajectory cluster was annotated using the ratio of female to male trajectories; however, it is important to remember that the sex of the trajectory was not used by the clustering algorithm (Fig. 3B). The cluster trajectories illustrated a range of sex biases and developmental patterns that included monotonic increases or decreases (e.g. clusters F30:M70 and F36:M64(1), respectively) but most trajectories were non-linear undulating waves of gene expression, and the clusters identified peaks and troughs at different ages across the lifespan (e.g. F100:M0, F13:M87)(Fig. 3B).

First, we assessed the clusters for sex differences. The Sex Bias Index (SBI) was calculated for each of the 25 clusters (SBI = +1 only female trajectories, 0 equal number of male and female trajectories, -1 only male trajectories). The SBI values ranged from 1 to -0.91, indicating that female trajectories dominated some clusters, some clusters had both sexes, and male trajectories dominated others (Fig. 4A).

One of the undulating clusters was exclusively female (SBI=1.00, F100:M0), with a peak in childhood and a trough in adolescence, while two clusters with opposite-phase undulations were strongly male-biased (SBI= -0.79, F13:M87; SBI= -0.91, F4:M96). Undulating waves were also found for clusters containing similar numbers of female and male trajectories (e.g. F47:M53, F36:M64(3)). Overall, 7 clusters had more female than male trajectories (SBI range 1.00 to 0.23), 10 had a roughly equal number of male and female trajectories (SBI range 0.14 to -0.18) and 8 had more male than female trajectories (SBI range -0.24 to -0.91).

To further examine the sex differences, we compared trajectories from the 2 female-biased clusters with the 2 male-biased clusters by calculating the ages when local maxima were reached. Both female- and male-biased clusters had one strongly undulating trajectory; however, the peak was earlier for males (F13:M87) at ~2 yrs and slightly later at 3 yrs

for females (F100:M0) (Fig. 4B). In addition, the two other strongly sex-biased clusters had trajectories that were opposite; the female-biased trajectory (F97:M3) declined through childhood, while the male-biased trajectory (F4:M96) increased (Fig. 4B). To determine the ages when gene expression had a local peak we calculated the local maxima for all 2010 trajectories and plotted a frequency histogram (Fig. 4C). Most peaks in gene expression occured in childhood (0-4 years) with a smaller fraction of trajectories showing an additional peak in older adults at 60-70 years of age.

Next, we examined the composition of the clusters and calculated Venn diagrams to compare which genes and brain areas gave rise to the trajectories in each cluster. We were surprised to find little overlap between female and male gene/brain area trajectories within a cluster (Fig. 5). In fact, 9 clusters had no overlap between the female and male gene/brain area trajectories. Despite the lack of overlap between the sexes, most clusters broadly represented the 15 brain areas (Fig. 6) and 10 virus families (Fig. 7). The 2 exceptions were male-biased clusters (F13:M87, F4:M96) that represented a smaller number of brain areas, with the majority of gene/brain area trajectories from the A1C and MD.

Those trajectory analyses identified a complex pattern of spatiotemporal development for the ssRNA virus receptors in the human brain. That development included a range of non-linear undulating developmental trajectories and a substantial number of sex differences across all brain areas and virus families.

Range of sexual dimorphism among the virus families

The next set of analyses assessed sex differences for the virus receptor genes within each of the 10 virus families (Supplementary Material Fig. 2). Cluster analysis of the trajectories for each virus family was done as described above for the whole dataset. Once again, each of the 10

virus families had a range of different gene/brain area trajectories, some with monotonic increases or decreases, but most clusters identified undulating trajectories of gene expression across the lifespan (Fig. 8). In addition, inspection of the Venn diagrams analyzing the composition of each cluster showed little overlap between the female and male gene/brain area trajectories in a cluster (Fig. 9). Overall, the clusters for each virus family represented trajectories from most of the brain areas (Fig. 10). However, there was more variation in the range of virus species found in each cluster, with some clusters having trajectories from just 1 or 2 virus species (Fig. 11).

Inspection of the SBI for the clusters in each virus family identified a range of sex biases from female-only to male-only (Fig. 12A-J). We noticed that some virus families had more sex-biased clusters, so to compare among the virus families, we calculated a sex Dimorphism Score (DS) for each family and plotted the distribution (Fig. 12K). The DS represented the overall sex bias for each family and had a value of 1 if all clusters had data from only one sex and 0 if there was an equal number of female and male trajectories in all clusters. The DS values ranged from a moderate dimorphism of DS=0.3 for the *Flaviviridae* family to strong dimorphism of DS=0.67 for the *Pneumoviridae* family. The next section examines the pattern of development and sex differences for each virus family from least to most sexually dimorphic.

Flaviviridae (DS=0.30)

The *Flaviviridae* viruses are primarily transmitted via arthropods (e.g., mosquitoes) and can cause symptoms from mild fever and malaise to fatal encephalitis and hemorrhagic fever (Eckels and Putnak, 2003; Wiley and Chimelli, 2017). Cluster analysis of the 18 *Flaviviridae* receptor genes identified 9 clusters, most with undulating trajectories; the smallest cluster had 19 trajectories, while the largest cluster had 118 trajectories (Fig. 8A). Two clusters were

female-biased, while the rest had a similar number of female and male trajectories, however, there was little overlap between the female and male gene/brain area trajectories (Fig. 9A). All clusters had a broad representation of brain areas and virus species (Figs. 10A & 11A). The virus receptor genes for this family were also broadly represented across the clusters, except clusters F47:M53(2), which was dominated by trajectories for TFRC, a receptor for the Hepacivirus C virus (Supplementary Material Fig. 2F).

Arenaviridae (DS= 0.33)

The *Arenaviridae* viruses are predominantly rodent-borne and cause diseases from mild febrile illness to severe hemorrhagic fever, with some, like the lymphocytic choriomeningitis virus causing nervous system disorders such as aseptic meningitis and encephalitis (Kibenge, 2016). We found 8 clusters for the *Arenaviridae* receptor gene trajectories; the smallest cluster had 12 trajectories, while the largest cluster had 53 trajectories (Fig. 8B). Most of the clusters had a similar number of female and male trajectories; however, 1 cluster had only female trajectories, and another was strongly male-biased (Fig. 9B). Interestingly, those sex-biased clusters represented the same virus species, Lymphocytic choriomeningitis mammarenavirus and Latino mammarenavirus (Fig. 10B), but the trajectories were out of phase, with females peaking in childhood and males in adults. Finally, the female-only cluster had most of the AXL trajectories (Supplementary Material Fig. 2F).

Filoviridae (DS= 0.42)

Filoviridae viruses can be transmitted via infected bodily fluids and are often fatal. The first symptoms, including hemorrhagic fever and gastrointestinal distress, lead to altered mental status, seizures and meningoencephalitis (Billioux, 2017). Lifespan trajectories were made for females and males using trajectories for the 8 *Filoviridae* receptor genes from the 15 brain areas.

Cluster analysis identified 8 trajectory clusters with a range of developmental patterns; the smallest cluster had 14 trajectories, while the largest cluster had 42 trajectories (Fig. 8C). Two of the clusters had only female trajectories, 4 had roughly equal numbers of female and male trajectories, and 2 clusters were male-biased (SBI= -0.29; females=15, males=27; SBI= -0.68; females=5, males=26).

Similar to the other virus families, there was little overlap between the gene/brain areas of the trajectories for females and males (Fig. 9C), and each cluster broadly represented the brain areas (Fig. 10C) and virus species (Ebola and Marburg viruses)(Fig. 11C). However, the virus receptor genes were not broadly represented across the clusters. For example, the 2 female-only clusters were dominated by different genes, MERTK and AXL vs CD209 (Supplementary Material Fig. 2F).

Orthomyxoviridae (DS=0.43)

Orthomyxoviridae viruses are predominantly respiratory pathogens that transmit through close personal contact. They generally cause mild symptoms such as fever, cough, sore throat, nasal congestion, body aches, headaches, chills, fatigue, and occasionally, diarrhea and vomiting. However, children are particularly prone to serious neurological complications like encephalopathy and febrile seizures (Surana et al., 2011). We clustered the trajectories for the 7 *Orthomyxoviridae* receptor genes and 15 brain areas resulting in 7 clusters with a range of developmental patterns; the smallest cluster had 21 trajectories, while the largest cluster had 42 trajectories (Fig. 8D). Two clusters were female-biased, 2 had a roughly equal number of female and male trajectories, and 3 were male-biased. Once again, there was little overlap between the gene/brain area of the trajectories for females and males (Fig. 9D) but a broad representation of

brain areas in each cluster (Fig. 10D). Interestingly, the strongly male-biased cluster was dominated by the receptor for the Influenza A virus, CD74 (Fig. 11D).

Rhabdoviridae (DS= 0.45)

Rhabdoviridae viruses are primarily zoonotic and include rabies and vesiculoviruses. The early stages of infection can be non-specific and flu-like, including fever, headache, and fatigue. However, severe neurological symptoms appear if the infection progresses, leading to seizures, delirium, paralysis and death (Schnell et al., 2010). Clustering of the *Rhabdoviridae* receptor genes for each brain area identified 5 different developmental trajectories; the smallest cluster had 24 trajectories, while the largest cluster had 44 trajectories (Fig. 8E). The 5 clusters had a range of trajectory patterns and sex bias from strongly female-biased (SBI=0.94) to male-biased (SBI=0.78)(Fig. 12E). There was a modest overlap between the female and male trajectories in 4 of the clusters (Fig. 9E) and a broad representation of brain areas in all clusters (Fig. 10E). The one strongly female-biased cluster peaked during adolescence, and most trajectories were receptors for the rabies virus (Fig. 11E), suggesting that the female brain may be more susceptible to rabies during adolescence.

Picornaviridae (DS= 0.48)

Picornaviridae viruses are transmitted via the fecal-oral route, respiratory route, or direct contact with infected individuals and cause a range of diseases, including the common cold, poliomyelitis, meningitis, hepatitis, and paralysis (Zell, 2018). Clustering of the 18 receptor genes for this family identified 11 clusters; the smallest cluster had 18 trajectories, and the largest 85 trajectories (Fig. 8F). The clusters had a range of SBI values (SBI= +1.00 to -0.64)(Fig. 12F) and little overlap between the female and male gene/brain trajectories (Fig. 9F). Interestingly, at either end of the SBI spectrum, the two strongly female-biased clusters and two strongly

male-biased clusters, had opposite trajectories. All of the clusters had a broad representation of brain areas and virus species (Coxsackievirus A, Coxsackievirus B, Echovirus E, Encephalomyocarditis virus, Enterovirus A, Enterovirus B, Enterovirus C, Enterovirus D, Hepatovirus A, Human enterovirus, Human parechovirus, Human rhinovirus A, Rhinovirus B, Rhinovirus C) highlighting the potential for brain-wide impact of sex differences in the development of virus receptors (Figs. 10F & 11F). For example, the female-only cluster was dominated by CD55, which regulates the complement system and is a receptor for 4 of the *Picornaviridae* family viruses (Supplementary Material Fig. 2F).

Coronaviridae (DS= 0.51)

Coronaviridae family viruses, including SARS, MERS and SARS-CoV-2, can cause highly infectious respiratory diseases with mild to severe symptoms. These viruses are known trigger a variety of neurological symptoms from headaches and loss of taste and smell to delirium, strokes, and long-term cognitive impairment (Spudich and Nath, 2022). Trajectories were made for the 25 *Coronaviridae* family genes in each brain area for females and males, and 12 clusters were identified. The smallest cluster had 16 trajectories, and the largest cluster had 121 trajectories (Fig. 8G).

The SBI values for the clusters ranged from 0.95 to -0.89, with half the clusters having strong sex bias (Fig. 12G) and 7 of the clusters having no overlap between female and male gene/brain area trajectories in the cluster (Fig. 9G). The 2 strongly female-biased clusters (F97:M3(1), F97:M3(2)) had trajectories that decreased in childhood and then increased through adolescence and adulthood. While the 2 strongly male-biased clusters (F19:M81, F6:M94) had more undulating trajectories that increased in childhood and then decreased across the rest of the lifespan. Furthermore, trajectories from particular brain areas dominated the strongly sex-biased

clusters (Fig. 10G). For example, half the trajectories in F97:M3(1) were from subcortical brain areas (AMY, MD, HIP, CBC), while the male-biased cluster with undulating trajectories (F18:M89) was dominated by data from A1C and AMY. It was unusual to find clusters dominated by such a small number of brain areas. In contrast, there was a fairly broad representation of the various receptor genes in each of the clusters (Fig. 11G).

Togaviridae (DS= 0.53)

The *Togaviridae* viruses are primarily transmitted via arthropod vectors (e.g., mosquitoes and ticks) and close personal contact. They cause a range of symptoms depending on host factors and the specific virus species, and common symptoms include arthralgia, headache, nausea, fever, seizures, confusion and photophobia (MacLachlan and Dubovi, 2011). We clustered the trajectories for the 4 *Togaviridae* genes in the 15 brain areas and identified 6 trajectory clusters (Fig. 8H). The smallest cluster had 11 trajectories, while the largest had 34 trajectories.

Only one of the clusters had an even representation of female and male trajectories, while the other 5 were sex-biased (Fig. 12H). Interestingly, the cluster with a balanced representation was the only cluster with an undulating trajectory pattern. Similar to the other virus families, the clusters had little or no overlap between the female and male gene/brain area trajectories (Fig. 9H) and most clusters had a broad representation of cortical and subcortical areas except the F91:M9 cluster that had only 8 brain areas and the largest proportion were subcortical (Fig. 10H). There was a range of virus species represented in the clusters (Fig. 11H), notably, the most sex-biased clusters were dominated by the same receptor genes (RPSA and MXRA8)(Supplementary Material Fig. 2F), but the clusters had opposite trajectories declining through childhood for females and increased in childhood before declining in adults for males.

Paramyxoviridae (DS= 0.62)

Viruses in the *Paramyxoviridae* family are primarily transmitted via respiratory routes or through contact with infected animals or food and drink. They cause a range of symptoms depending on the specific virus species and host factors such as age or underlying conditions, including fever, cough, headache, encephalitis and meningitis (Norrby and Kristensson, 1997; Goh et al., 2000; Wong et al., 2009). Clustering the trajectories for the 5 receptors for the *Paramyxoviridae* family produced 6 clusters of varying sizes: the smallest cluster had 12 trajectories, and the largest cluster had 59 trajectories (Fig. 8I). Half of the clusters were strongly female-biased (SBI= 0.83 to 0.75), and the other half were moderately male-biased (SBI= -0.15 to -0.58)(Fig. 12I). There was little overlap between a cluster's female and male gene/brain trajectories (Fig. 9I). The trajectories had a range of shapes, including undulating trajectories for female- and male-biased clusters (Fig. 8I). The female-biased undulating trajectory was dominated by CD46 (Supplementary Material Fig. 2F). That receptor participates in the regulation of the complement system and is used by the measles virus to gain cell entry and dampen the complement-mediated immune response.

Pneumoviridae (DS=0.67)

The most well-known members of the *Pneumoviridae* family are the human respiratory syncytial virus (HRSV) and human metapneumovirus (HMPV), which primarily infect the respiratory tract and are transmitted via close personal contact and suspension droplets (MacLachlan and Dubovi, 2011). Individuals infected by these viruses present with flu-like symptoms, bronchitis, febrile or afebrile seizures, status epilepticus, encephalopathies and encephalitis (Bohmwald et al., 2018b). Clustering of the 5 *Pneumoviridae* receptor genes (Supplementary Material Table 2) identified 7 trajectory clusters; the smallest cluster had 8

trajectories, while the largest cluster had 41 trajectories (Fig. 8J). This virus family had the strongest sexual dimorphism: only 1 cluster had an equal number of female and male trajectories, while the other 6 clusters were strongly biased, with 2 clusters that had only female trajectories, 2 were strongly female-biased, 1 with only male trajectories, and 1 was strongly male-biased (Fig. 12J). Furthermore, there was minimal overlap between the genes/brain areas of the female and male trajectories in the clusters (Fig. 9J).

All of the *Pneumoviridae* clusters had non-linear undulating patterns that included a broad range of brain areas except cluster F100:M0(1) that only had cortical areas (Fig. 10J). Interestingly, the 2 clusters with female-only trajectories had different developmental patterns and virus species – one increased through childhood (F100:M0(1)) and only had 1 virus receptor (ITGB1) for HMPV, while the other (F100:M0(2)) decreased through childhood and only had virus receptors for HRSV (CD209, CLEC4M and CX3CR1)(Figs. 11J & Supplementary Material Fig. 2F).

Differential gene analysis identified brain-wide patterns of early sex differences

To identify sex- and age-specific differential expression of the 67 virus genes in the 15 brain areas, we applied the sliding window differential gene expression analysis, DE-SWAN (Lehallier et al., 2019), and visualized the results as heatmaps. Cells in the heatmaps were colour-coded purple when females expressed more and green when males expressed more of the gene (Fig. 13). The heatmaps have a row for each virus receptor gene and a column for each of the 13 reference ages. The order of the rows was arranged with a dendrogram to cluster genes with similar patterns of sex- and age-related differential gene expression.

First, we compared the overall pattern of the sex- and age-related differences among the 15 brain areas (Fig. 13A-O). It is important to note that the x-axes on the heatmaps are not

linear, and the first 8 columns represent ages from 6 months to 12 years while the last 5 columns represent ages from 16 to 80 years. Visual inspection of those plots highlighted a common pattern with many purple and green coloured cells occurring during childhood (left half of each heatmap) and fewer coloured cells in adulthood (right side of the heatmaps) signifying that there are more sex differences in the developing brain than in adults (Fig. 13). In addition, in adults there was more variability among the brain areas in the number of genes with differential expression between females and males. For example, in older adults almost half of the genes in the DFC had differential expression with some higher in females and others higher in males. In contrast, V1C had relatively few genes with differential expression in adults. Thus, the DE-SWAN analysis identified a brain-wide pattern of sex differences where the majority of differences occurred before puberty.

Next, we focused on addressing if those patterns of sex- and age-related virus receptor gene expression provide insights into common neurological complications associated with viral infections. Viral diseases can cause a diverse range of neurological symptoms and outcomes and the families studied have 3 major categories: neuroinflammation, sensory-motor deficits, and cognitive impairment. Sex differences have been described for some of those categories (Thompson et al., 2005; Weatherhead et al., 2015; Rubin et al., 2019; Romagnolo et al., 2021; Savarraj et al., 2021; Evans et al., 2022), and here we explored if the sex- and age-related patterns of virus receptor gene expression revealed by the DE-SWAN analysis help to understand the biological basis of symptom-related sex differences. This section concentrates on the DE-SWAN analysis of 2 cortical areas (DFC, A1C) and one subcortical area (HIP) most closely associated with neurological symptoms and outcomes caused by viral infections.

Neuroinflammation: Common complications of viral infections include encephalopathy, encephalitis, and meningitis, all of which involve neuroinflammatory processes. For example, about 1 in 150 people infected with the West Nile virus (WNV), a member of the *Flaviviridae* family, develop encephalitis with males being more susceptible to neuroinvasive symptoms (Carson et al., 2012; James et al., 2016; Yeung et al., 2017; Riccetti et al., 2023).

The 4 receptors for WNV, CD209, CLEC4M, ITGAV, ITGB3 (Fig. 14, blue arrows) show a pattern of sex differences in childhood with fewer differences in young or older adults in DFC, A1C or HIP (Fig. 14). In the DFC 3 of the 4 receptors (CD209, CLEC4M, ITGB3) had higher expression in infant females but switched to higher expression in male children (Fig. 14A). In contrast, in the A1C, 3 of the 4 receptors (CD209, CLEC4M, ITGB3) had higher expression in male children and for CD209 that extended through adolescence (Fig. 14B). In the HIP, CD209 and ITGAV had higher expression in female infants and children while CLEC4M and ITGB3 had higher expression in male children (Fig. 14C). In adults, the genes with differential expression all had higher expression in females, including CD209 and CLEC4M in DFC, ITGAV and ITGB3 in A1C, and CLEC4M and ITGAV in HIP. Thus, the pattern of sex- and age-related differential expression of the WNV receptor genes in these brain areas does not provide new insights into greater susceptibility of adult males to neuroinvasive symptoms.

Sensory motor deficit: Sensory-motor deficits encompass a range of neurological complications caused by viral infections, leading to symptoms such as paralysis, seizures, tinnitus, anosmia, balance and proprioception. These deficits are observed in individuals infected by various viruses, including the Enterovirus (EV) and the Rabies virus (RABV).

One of the prominent receptors for EV is SCARB2 (Fig. 14, orange arrow), which is involved in cellular processes such as lysosomal targeting and neuron repair and development

(Kobayashi and Koike, 2020). Furthermore, the distribution of SCARB2 is correlated with pathological changes observed after infection with the Enterovirus (Jiao et al., 2014). Two receptors for the RABV, NGFR and NCAM1 (Fig. 14, orange arrows), are essential factors regulating central nervous system growth and development and are widely expressed in the brain. Once inside the cell, RABV is readily transported from neuron to neuron, causing dysregulation of the cytoskeleton and neurodegeneration (Liu et al., 2022). All of these receptors had age- and sex-related differential expression and some variation among the brain areas. In the DFC, SCARB2 and NGFR had similar patterns of sex differences with higher expression in infant females, shifting to higher expression in older male children and then back to higher expression in females through adulthood (Fig. 14A). In A1C and HIP, both SCARB2 and NGFR had higher expression in young female children (Fig. 14 B&C). For SCARB2, that higher female expression extended through adolescence in A1C and returned in older female adults in HIP. In contrast with the female-dominated patterns for SCARB2 and NGFR, the expression of NCAM1 had higher expression in infant males in the DFC and A1C that shifted to higher female expression in older children (Fig. 14 A&B). In the HIP, NCAM1 had higher expression in adolescent females (Fig. 14C). The high mortality caused by RABV continues to be a significant public health concern (Kumar et al., 2023). These patterns of age- and sex-related differences in virus receptor expression in the human brain may provide some insights into vulnerability to infection and sex-specific treatments.

Cognitive Impairments: Many viral infections cause cognitive deficits that can be acute or longer-lasting and include symptoms such as "brain fog" characterized by difficulties in organizing thoughts, multitasking, and problem-solving. Additionally, individuals may experience memory problems, executive function challenges, and cognitive fatigue, collectively

impacting their cognitive abilities and overall cognitive performance. Two common viruses that have these symptoms are the SARS-CoV-2 virus (Soriano et al., 2022), a member of the *Coronaviridae* family, and the Influenza A virus (IAV) (Hosseini et al., 2018), a member of the *Orthomyxoviridae* family.

All of the 7 SARS-CoV-2 receptors (ACE2, ADAM17, AXL, CTSL1, FURIN, NRP1, SCARB1)(Fig. 14, grey arrows) had sex- and age-related differential gene expression, but the pattern of sex differences differed between the cortical and subcortical areas. In the DFC and A1C, the sex differences were dominated by higher female expression (Fig. 14 A&B). Still, in the HIP, most of the sex differences were dominated by males (Fig. 14C). Only one receptor, ACE2, did not follow that pattern and had more expression in the DFC of older males and the A1C of males from infancy through adolescence, but weak differential expression in the HIP. In addition, many integrin co-factors that facilitate cell entry of the SARS-CoV-2 virus had higher expression in adult females. The one exception was ITGA2, which had higher expression in adult males in the DFC, A1C and HIP. The higher expression of the integrins, especially in adult females, is interesting because that may contribute to some long-COVID symptoms by enhancing invasion of SARS-CoV-2 in the brain.

The 7 IAV receptors (ANXA5, CACNA1C, CD209, CD74, CLEC4M, EGFR, UVRAG)(Fig. 14, grey arrows) tended to have higher expression in female infants and young children. For example, in the DFC, all 7 genes had higher expression levels in young females, but 4 of them (ANXA5, CD209, CD74, UVRAG) switched to higher expression in older male children (Fig. 14A). We found different patterns of sex differences in A1C and HIP. In A1C, 3 receptors (CACNA1C, CD209, CLEC4M) had higher expression levels in very young males. At the same time, the other 4 had higher expression in young females (Fig. 14B). In HIP, 2 IAV

receptors (CACNA1C, EGFR) had higher expression in young males, 4 receptors (ANXA5, CD74, CLEC4M, UVRAG) had higher expression in adolescent males and 3 in adult males (CACNA1C, CD74, UVRAG)(Fig. 14C). These complex patterns differed among these 3 brain areas and suggested that considering the age, sex and the brain areas associated with the specific cognitive symptoms are important for understanding the neural basis of deficits caused by IAV infection.

Together, the DE-SWAN analyses revealed complex patterns of virus receptor sex differences at distinct stages of life, with many genes having differential expression during childhood and adolescence. Furthermore, we highlighted particular gene- and brain-area-specific patterns that might be associated with neurological complications accompanying some viral infections.

Sex-specific virus receptor development in the cortex

Finally, we analyzed the overall high-dimensional developmental patterns among the 15 brain areas for both sexes. For these analyses, the data frame was reorganized to focus on studying the development of the brain areas. That involved making a matrix with 30 rows, one for each brain (n=15) area and sex (n=2), and 8576 columns for the 128 LOESS fitted values for each of the 67 genes. Then we applied unsupervised hierarchical clustering to determine if the high dimensional pattern of brain-wide development would reveal groups of brain areas with similar development.

The cluster analysis identified 4 groups, including 2 large clusters with most brain areas but almost exclusively just 1 sex: one cluster with male-only data; one with mostly female data except for the male HIP data (Fig. 15A). The other 2 small clusters had both sexes and data from the CBC or MD. Thus, even this optimized analysis found little evidence for brain area-specific

development and instead highlighted that sex was the strongest driver of diversity in the data for most brain areas.

To further unpack these clusters, we applied tSNE visualization (denstsne in R) to provide a 2D representation of the high dimensional information about virus receptor development in the human brain. Colour-coding the tSNE plot for the 4 clusters showed good segregation (Fig. 15B), but adding colour-coding for age (Fig. 15C) did not reveal an overall pattern. Instead, colour-coding the data for sex and cortical vs subcortical showed an obvious sex-specific pattern (Fig. 15D). The trajectories for the 11 cortical areas were separated by sex on the tSNE plot, while the 4 subcortical areas (AMY, HIP, MD, CBC) for females and males were either adjacent to or nearby in the plot. The spatial separation of the female and male cortical areas supports the conclusion that virus receptor development in the human cortex follows distinct sex-specific programs. Furthermore, those programs are not simple shifts where one sex develops earlier than the other but instead they are unique development patterns.

Discussion

This study characterized the sex-specific development of 67 ssRNA virus receptor and co-factor genes in the human brain. We applied high-dimensional analyses of the developmental trajectories for the virus genes in each brain area. Most trajectories have non-linear changes across the lifespan, including undulating trajectories. Surprisingly, there was little overlap between the sexes in the developmental trajectories for each gene in the brain areas. Further analysis showed that all 10 virus families had sex-specific development. Still, there was a range of sexual dimorphism among the virus families, with the *Pneumoviridae* family having the most distinct difference between the development of females and males. By applying a sliding window differential gene analysis (DE-SWAN) to each of the 15 brain areas, we identified that most sex differences occurred in childhood before puberty. Notably, the disparity in virus receptor gene development between females and males was most distinct in the cortex, where the 2 sexes followed unique trajectories.

The gene- age- and sex-specific patterns found here may help to understand certain neurological symptoms associated with viral infections. For example, a prevalent view is that the immune response in females contributes to their better outcomes after infection (Scully et al., 2020; Takahashi et al., 2020b). Our findings suggest that age- and sex-specific expression of virus receptors in the human brain may also contribute to sex differences in severity, comorbidity and presentation of neurological symptoms caused by neurotropic viral infections. That notion is consistent with observational data that the sex bias in disease outcomes is age- and virus-specific (Peretz et al., 2015) and the absence of a host factor can impede or prevent infection while an increased presence can enhance infection (Song et al., 2021a; Martínez-Mármol et al., 2023b). Thus, our characterization of age- and sex-specific expression of virus receptors in the human

brain identifies additional factors that may contribute to the vulnerability and variability of neurological symptoms caused by viral infection.

We designed this study to assess age- and sex-related differences in virus receptor development in the human brain. We applied a sensitive bioinformatics approach for assessing non-linear developmental patterns (Lehallier et al., 2019, 2020). In our study, we used LOESS regression models to trace lifespan trajectory patterns that followed the non-linear pattern of gene expression. That trajectory analysis takes advantage of all the data and does not force cases into predefined age bins that may not be appropriate for both sexes. Additionally, the unsupervised clustering effectively revealed differences among trajectories without any *a priori* knowledge about the sex, gene, or brain area. However, like all studies using the rare and valuable resources of developmental postmortem brain tissue, this study had a limited number of cases to analyze. To help with mitigating that limitation we used the most extensive transcriptomic database available (Kang et al., 2011) and adopted this modern data-driven approach using sensitive analyses for describing the non-linear developmental patterns. We were surprised when those patterns revealed so many sex differences. Those sex differences reflect population-level changes in gene expression but may provide a framework for understanding individual differences in the impact of viral infections at different stages of the lifespan.

It is important to recognize that other factors such as gender, socio-economic status and access to healthcare contribute to differences in the impact of viral infections on females and males. However, that information is not collected by the brain banks. In addition, our study used transcriptomic data from individuals who died from accidents and a range of diseases, so it is impossible to tease apart the impact of the different causes of death. Nevertheless, the design

of our study, the use of an extensive database, and the application of sensitive trajectory analyses provide a new understanding of virus-related sex differences in the human brain.

Sex differences within virus families and brain areas

The diversity of trajectories and lack of overlap between females and males for each virus family and brain area highlights the complex molecular environment for viral infections in the human brain. The cluster analysis showed that the various trajectory patterns included multiple genes, brain areas and virus species. However, they did not equally represent the two sexes. All of the virus families had at least 1 trajectory pattern that was strongly or exclusively female and most had a trajectory dominated by males. Since there are virus-specific sex biases in disease outcomes, we examined if sex biases in virus receptor expression were linked to specific virus species. Most of the sex biased trajectories represented multiple virus species but a few were dominated by or exclusive to 1 virus species. For example, the two female-only trajectories for the *Pneumovirdae* family represented receptors for different virus species. The trajectory that increased included receptors for the human metapneumovirus (HMPV) while the trajectory that decreased included receptors for the human respiratory syncytial virus (HRSV). Those findings may help to clarify the mechanisms that cause neurological complications in females after HMPV versus HRSV viral infections.

Previous studies found that WNV-infected females report more symptoms than WNV-infected males, but in the United States, males infected with WNV have higher rates of hospitalization and occurrence of neuroinvasive disease (Curren et al., 2018; Hoffman et al., 2019). Furthermore, hearing loss is one of the expected long-term outcomes of WNV infection (Weatherhead et al., 2015). Age is another factor in WNV, where neuroinvasive infection is more common in older adults, but it does occur in the pediatric population (Herring et al., 2019).

Unfortunately, there is little information about sex differences in children's symptoms with neuroinvasive WNV infections. The current findings about WNV receptor expression in children, where some have higher expression in females and others in males, will spur interest in examining if girls and boys have different outcomes after WNV infection.

One of the striking sex differences was the complete separation of virus receptor development in the cortical areas between females and males. Females are often described as developing precociously relative to males, but our findings paint a different picture. Instead, the high-dimensional analysis of all 67 receptors in the cortical areas showed that females and males have distinct developmental trajectories. They are not simply age-shifted; rather, the cortex of females and males have different molecular environments for virus receptors. This finding has broad implications for understanding the pathophysiology of neurological symptoms caused by viral infections.

The majority of sex difference occur before puberty

Most sex differences in virus gene expression were found between birth and 10 to 12 years, before puberty. That timing stresses the importance of collecting high-quality sex-disaggregated data about the neurological impact of viral infection in children. Also, it highlights the need to explore more targeted treatments for viral infections in children. Those findings raise questions about the long-term impact of viral infection on brain development since the sex differences occur during rapid development and refinement of circuits in the brain. For example, inflammation caused by viral infections in the developing brain increases the risk of cerebral palsy, autism spectrum disorders, schizophrenia, multiple sclerosis, cognitive impairment, and Parkinson's disease (Hagberg et al., 2012; al-Haddad et al., 2019). The sex differences identified in our study provide a starting point to address the sex-specific impact of

molecular mechanisms used by viruses to cause inflammation in the developing brain. Furthermore, those molecular differences may contribute to the prevalence of certain post-infection disorders observed in older children, teens and adults.

Viral infections may have sex-specific neuroinvasive impact in children

Many studies have examined the neuroinvasive impact and resulting pathology of viral infections (Koyuncu et al., 2013). However, the COVID-19 pandemic has increased the need to understand the mechanisms underlying the neuroinvasive potential of viral agents and the subsequent acute and post-acute neurological manifestations. The need is particularly true for respiratory transmitted viruses as these infections contribute significantly to yearly morbidity and mortality rates impacting vulnerable populations such as young children, older adults, and individuals with weakened immune systems. In addition, they have different morbidity and mortality rates between females and males (Bohmwald et al., 2018b; Tsai et al., 2021; Pelà et al., 2022). While acknowledging the variability in morbidity and mortality between sexes, it is worth noting that the extent of this variability can be influenced by complicated interaction between the host, virus and environment (Peretz et al., 2015; Kumar et al., 2021b; Samadizadeh et al., 2021). Our findings shed light on overlooked sexual dimorphisms in the molecular mechanisms used by respiratory virus families and may inform prevention and management strategies for infected individuals, including asymptomatic cases that can still have long-term neurological complications.

Model systems to study sex differences in the impact of viruses on the brain

Various animal models and, more recently, brain organoids are used to understand disease progression, pathogenesis, and host immune responses to neuroinvasive viruses. For COVID-19

research, several transgenic mice models engineered with human ACE2 (hACE2) simulate varying aspects of the disease, from lethal to non-lethal infections (Muñoz-Fontela et al., 2020). Those studies revealed the neural impact of the SARS-CoV-2 virus on both neurons and non-neuronal cells in the brain (e.g., (Song et al., 2021b; Fernández-Castañeda et al., 2022), including fusion of neurons and glial cells into syncytia with pathological function (Martínez-Mármol et al., 2023a). Furthermore, studies using non-human primates showed the neuroinvasive potential of SARS-CoV-2, and that neuronal damage is greater in older animals (Beckman et al., 2022). Additionally, brain organoids have provided invaluable insights into the neuroinvasive potential of the SARS-CoV-2, Zika, and Dengue virus (Abreu et al., 2018; Sutarjono, 2018; Pellegrini et al., 2020; Song et al., 2021a; Martínez-Mármol et al., 2023b).

The over-representation of male animals is a significant shortcoming in understanding the mechanisms contributing to sex-specific symptoms and outcomes of viral infection. Nevertheless, when animal studies are designed to examine the impact of sex on viral infections, they often identify key differences (Barna 1996,Wynne 2011,Snyder-Keller 2019,Yirrell 1987,Yan 2021). An ideal animal model should explore a range of host-virus interactions that would facilitate the translational potential of preclinical studies.

In conclusion, our study identified a complex spatiotemporal pattern of sex differences in developing ssRNA virus receptors in the human brain. Surprisingly, most sex differences occurred before puberty and were most robust in the cortex.

Viral receptors are the first line of interaction and the spatiotemporal expression of the receptors plays a key role in understanding the pathogenesis of various infectious symptoms. Identifying the precise timing of receptor differences in males and females provides invaluable insight, guiding us toward developing more effective treatments. We hope the sex differences

identified here will serve as a call to action for future studies into the neuroinvasive impact of viruses.

References

Aaby P, Bukh J, Hoff G, Lisse IM, Smits AJ (1986) Cross-Sex Transmission of Infection and Increased Mortality Due to Measles. Clin Infect Dis 8:138–143.

Abreu CM, Gama L, Krasemann S, Chesnut M, Odwin-Dacosta S, Hogberg HT, Hartung T, Pamies D (2018) Microglia Increase Inflammatory Responses in iPSC-Derived Human BrainSpheres. Front Microbiol 9:2766.

Alt H, Godau M (1995) Computing the Frechet Distance Between Two Polygonal Curves. Int J Comput Geom Appl 05:75–91.

Beckman D, Bonillas A, Diniz GB, Ott S, Roh JW, Elizaldi SR, Schmidt BA, Sammak RL, Rompay KKAV, Iyer SS, Morrison JH (2022) SARS-CoV-2 infects neurons and induces neuroinflammation in a non-human primate model of COVID-19. Cell Rep 41:111573.

Billioux BJ (2017) Neurological Complications and Sequelae of Ebola Virus Disease. Curr Infect Dis Rep 19:19.

Bohmwald K, Gálvez NMS, Ríos M, Kalergis AM (2018a) Neurologic Alterations Due to Respiratory Virus Infections. Front Cell Neurosci 12:386.

Bohmwald K, Gálvez NMS, Ríos M, Kalergis AM (2018b) Neurologic Alterations Due to Respiratory Virus Infections. Front Cell Neurosci 12:386.

Calin-Jageman RJ, Cumming G (2019) Estimation for Better Inference in Neuroscience. Eneuro 6:ENEURO.0205-19.2019.

Carson PJ, Borchardt SM, Custer B, Prince HE, Dunn-Williams J, Winkelman V, Tobler L, Biggerstaff BJ, Lanciotti R, Petersen LR, Busch MP (2012) Neuroinvasive Disease and West Nile Virus Infection, North Dakota, USA, 1999–2008 - Volume 18, Number 4—April 2012 -

Emerging Infectious Diseases journal - CDC. Emerg Infect Dis 18:684–686.

Cheng Q, Yang Y, Gao J (2020) Infectivity of human coronavirus in the brain. Ebiomedicine 56:102799.

Curren EJ, Lehman J, Kolsin J, Walker WL, Martin SW, Staples JE, Hills SL, Gould CV, Rabe IB, Fischer M, Lindsey NP (2018) West Nile Virus and Other Nationally Notifiable Arboviral Diseases — United States, 2017. Morb Mortal Wkly Rep 67:1137–1142.

Douaud G et al. (2022) SARS-CoV-2 is associated with changes in brain structure in UK Biobank. Nature 604:697–707.

Eckels KH, Putnak R (2003) Formalin-Inactivated Whole Virus and Recombinant Subunit Flavivirus Vaccines. Adv Virus Res 61:395–418.

Engin AB, Engin ED, Engin A (2021) Current opinion in neurological manifestations of SARS-CoV-2 infection. Curr Opin Toxicol 25:49–56.

Evans RA et al. (2022) Clinical characteristics with inflammation profiling of long COVID and association with 1-year recovery following hospitalisation in the UK: a prospective observational study. Lancet Respir Med 10:761–775.

Fernández-Castañeda A et al. (2022) Mild respiratory COVID can cause multi-lineage neural cell and myelin dysregulation. Cell 185:2452-2468.e16.

Giurgea LT, Cervantes-Medina A, Walters K-A, Scherler K, Han A, Czajkowski LM, Baus HA, Hunsberger S, Klein SL, Kash JC, Taubenberger JK, Memoli MJ (2021) Sex Differences in Influenza: The Challenge Study Experience. J Infect Dis 225:jiab422-.

Goh KJ, Tan CT, Chew NK, Tan PSK, Kamarulzaman A, Sarji SA, Wong KT, Abdullah BJJ, Chua KB, Lam SK (2000) Clinical Features of Nipah Virus Encephalitis among Pig Farmers in Malaysia. New Engl J Medicine 342:1229–1235.

Gujski M, Jankowski M, Rabczenko D, Goryński P, Juszczyk G (2021) Characteristics and Clinical Outcomes of 116,539 Patients Hospitalized with COVID-19—Poland, March–December 2020. Viruses 13:1458.

Herring R, Desai N, Parnes M, Jarjour I (2019) Pediatric West Nile Virus-Associated Neuroinvasive Disease: A Review of the Literature. Pediatr Neurol 92:16–25.

Ho J, Tumkaya T, Aryal S, Choi H, Claridge-Chang A (2019) Moving beyond P values: data analysis with estimation graphics. Nat Methods 16:565–566.

Hoffman KW, Lee JJ, Foster GA, Krysztof D, Stramer SL, Lim JK (2019) Sex differences in cytokine production following West Nile virus infection: Implications for symptom manifestation. Pathog Dis 77.

Hosseini S, Wilk E, Michaelsen-Preusse K, Gerhauser I, Baumgärtner W, Geffers R, Schughart K, Korte M (2018) Long-Term Neuroinflammation Induced by Influenza A Virus Infection and the Impact on Hippocampal Neuron Morphology and Function. J Neurosci 38:3060–3080.

Jacobsen H, Klein SL (2021) Sex Differences in Immunity to Viral Infections. Front Immunol 12:720952.

James EA, Gates TJ, LaFond RE, Yamamoto S, Ni C, Mai D, Gersuk VH, O'Brien K, Nguyen Q-A, Zeitner B, Lanteri MC, Norris PJ, Chaussabel D, Malhotra U, Kwok WW (2016) Neuroinvasive West Nile Infection Elicits Elevated and Atypically Polarized T Cell Responses That Promote a Pathogenic Outcome. PLoS Pathog 12:e1005375.

Jiao X-Y, Guo L, Huang D-Y, Chang X-L, Qiu Q-C (2014) Distribution of EV71 receptors SCARB2 and PSGL-1 in human tissues. Virus Res 190:40–52.

Kaeuffer C et al. (2020) Clinical characteristics and risk factors associated with severe COVID-19: prospective analysis of 1,045 hospitalised cases in North-Eastern France, March

2020. Eurosurveillance 25:2000895.

Kang HJ et al. (2011) Spatio-temporal transcriptome of the human brain. Nature 478:483–489.

Kibenge FSB (2016) Aquaculture Virology. Part : Gen Asp:9–34.

Klein SL, Flanagan KL (2016) Sex differences in immune responses. Nat Rev Immunol 16:626–638.

Klein SL, Hodgson A, Robinson DP (2012) Mechanisms of sex disparities in influenza pathogenesis. J Leukoc Biol 92:67–73.

Klein SL, Huber S (2009) Sex Hormones and Immunity to Infection Klein SL, Roberts C, eds. :93–122.

Kobayashi K, Koike S (2020) Cellular receptors for enterovirus A71. J Biomed Sci 27:23.

Koyuncu OO, Hogue IB, Enquist LW (2013) Virus Infections in the Nervous System. Cell Host Microbe 13:379–393.

Kumar A, Bhatt S, Kumar A, Rana T (2023) Canine rabies: An epidemiological significance, pathogenesis, diagnosis, prevention, and public health issues. Comp Immunol, Microbiol Infect Dis 97:101992.

Kumar A, Narayan RK, Kulandhasamy M, Prasoon P, Kumari C, Kumar S, Pareek V, Sesham K, Shekhawat PS, Kant K, Kumar S (2021) COVID-19 pandemic: insights into molecular mechanisms leading to sex-based differences in patient outcomes. Expert Rev Mol Med 23:e7.

Lehallier B, Gate D, Schaum N, Nanasi T, Lee SE, Yousef H, Losada PM, Berdnik D, Keller A, Verghese J, Sathyan S, Franceschi C, Milman S, Barzilai N, Wyss-Coray T (2019) Undulating changes in human plasma proteome profiles across the lifespan. Nature Medicine:1–22.

Lehallier B, Shokhirev MN, Wyss‐Coray T, Johnson AA (2020) Data mining of human plasma proteins generates a multitude of highly predictive aging clocks that reflect different aspects of

aging. Aging Cell 19:e13256.

Levine KS, Leonard HL, Blauwendraat C, Iwaki H, Johnson N, Bandres-Ciga S, Ferrucci L, Faghri F, Singleton AB, Nalls MA (2023) Virus exposure and neurodegenerative disease risk across national biobanks. Neuron 111:1086-1093.e2.

Liu X, Nawaz Z, Guo C, Ali S, Naeem MA, Jamil T, Ahmad W, Siddiq MU, Ahmed S, Idrees MA, Ahmad A (2022) Rabies Virus Exploits Cytoskeleton Network to Cause Early Disease Progression and Cellular Dysfunction. Front Vet Sci 9:889873.

Maaten L van der, Hinton G (2008) Visualizing Data using t-SNE. Journal of Machine Learning Research 9:2579–2605.

MacLachlan NJ, Dubovi EJ (2011) Fenner's Veterinary Virology (Fourth Edition). Part II: Vet Zoonotic Viruses:455–465.

Martínez-Mármol R, Giordano-Santini R, Kaulich E, Cho A-N, Przybyla M, Riyadh MA, Robinson E, Chew KY, Amor R, Meunier FA, Balistreri G, Short KR, Ke YD, Ittner LM, Hilliard MA (2023a) SARS-CoV-2 infection and viral fusogens cause neuronal and glial fusion that compromises neuronal activity. Sci Adv 9:eadg2248.

Martínez-Mármol R, Giordano-Santini R, Kaulich E, Cho A-N, Przybyla M, Riyadh MA, Robinson E, Chew KY, Amor R, Meunier FA, Balistreri G, Short KR, Ke YD, Ittner LM, Hilliard MA (2023b) SARS-CoV-2 infection and viral fusogens cause neuronal and glial fusion that compromises neuronal activity. Sci Adv 9.

Mauvais-Jarvis F, Merz NB, Barnes PJ, Brinton RD, Carrero J-J, DeMeo DL, Vries GJD, Epperson CN, Govindan R, Klein SL, Lonardo A, Maki PM, McCullough LD, Regitz-Zagrosek V, Regensteiner JG, Rubin JB, Sandberg K, Suzuki A (2020) Sex and gender: modifiers of health, disease, and medicine. Lancet 396:565–582.

Mavrikaki M, Lee JD, Solomon IH, Slack FJ (2022) Severe COVID-19 is associated with molecular signatures of aging in the human brain. Nat Aging 2:1130–1137.

Mishra R, Banerjea AC (2020) Neurological Damage by Coronaviruses: A Catastrophe in the Queue! Front Immunol 11:565521.

Morgan R, Klein SL (2019) The intersection of sex and gender in the treatment of influenza. Curr Opin Virol 35:35–41.

Morgello S (2020a) Coronaviruses and the central nervous system. J Neurovirol 26:459–473.

Morgello S (2020b) Coronaviruses and the central nervous system. J Neurovirol 26:1–15.

Muñoz-Fontela C et al. (2020) Animal models for COVID-19. Nature 586:509–515.

Murthy S et al. (2021) Characteristics and outcomes of patients with COVID-19 admitted to hospital and intensive care in the first phase of the pandemic in Canada: a national cohort study. CMAJ Open 9:E181–E188.

Narayan A, Berger B, Cho H (2021) Assessing single-cell transcriptomic variability through density-preserving data visualization. Nat Biotechnol 39:1–10.

Nath A, Johnson TP (2022) Mechanisms of viral persistence in the brain and therapeutic approaches. FEBS J 289:2145–2161.

Norrby E, Kristensson K (1997) Measles Virus in the Brain. Brain Res Bull 44:213–220.

Paniz‐Mondolfi A, Bryce C, Grimes Z, Gordon RE, Reidy J, Lednicky J, Sordillo EM, Fowkes M (2020) Central nervous system involvement by severe acute respiratory syndrome coronavirus‐2 (SARS‐CoV‐2). J Méd Virol 92:699–702.

Pellegrini L, Albecka A, Mallery DL, Kellner MJ, Paul D, Carter AP, James LC, Lancaster MA (2020) SARS-CoV-2 Infects the Brain Choroid Plexus and Disrupts the Blood-CSF Barrier in Human Brain Organoids. Cell Stem Cell 27:951-961.e5.

Peretz J, Hall OJ, Klein SL (2015) Sex and Gender Differences in Infection and Treatments for Infectious Diseases. :183–210.

Prado-Galbarro F-J, Sanchez-Piedra C, Gamiño-Arroyo AE, Cruz-Cruz C (2020) Determinants of survival after severe acute respiratory syndrome coronavirus 2 infection in Mexican outpatients and hospitalised patients. Public Heal 189:66–72.

Rao GG et al. (2021) Cross-sectional observational study of epidemiology of COVID-19 and clinical outcomes of hospitalised patients in North West London during March and April 2020. BMJ Open 11:e044384.

Riccetti N, Ferraccioli F, Fasano A, Stilianakis NI (2023) Demographic characteristics associated with West Nile virus neuroinvasive disease – A retrospective study on the wider European area 2006–2021. PLOS ONE 18:e0292187.

Romagnolo A, Balestrino R, Imbalzano G, Ciccone G, Riccardini F, Artusi CA, Bozzali M, Ferrero B, Montalenti E, Montanaro E, Rizzone MG, Vaula G, Zibetti M, Lopiano L (2021) Neurological comorbidity and severity of COVID-19. J Neurol 268:762–769.

Rosenthal N, Cao Z, Gundrum J, Sianis J, Safo S (2020) Risk Factors Associated With In-Hospital Mortality in a US National Sample of Patients With COVID-19. JAMA Netw Open 3:e2029058.

Rubin LH, Neigh GN, Sundermann EE, Xu Y, Scully EP, Maki PM (2019) Sex Differences in Neurocognitive Function in Adults with HIV: Patterns, Predictors, and Mechanisms. Curr Psychiatry Rep 21:94.

Samadizadeh S, Masoudi M, Rastegar M, Salimi V, Shahbaz MB, Tahamtan A (2021) COVID-19: why does disease severity vary among individuals? Resp Med 180:106356.

Savarraj J, Park ES, Colpo GD, Hinds SN, Morales D, Ahnstedt H, Paz AS, Assing A, Liu F,

Juneja S, Kim E, Cho S, Gusdon AM, Dash P, McCullough LD, Choi HA (2021) Brain injury, endothelial injury and inflammatory markers are elevated and express sex-specific alterations after COVID-19. J Neuroinflammation 18:277.

Schnell MJ, McGettigan JP, Wirblich C, Papaneri A (2010) The cell biology of rabies virus: using stealth to reach the brain. Nat Rev Microbiol 8:51–61.

Scully EP, Haverfield J, Ursin RL, Tannenbaum C, Klein SL (2020) Considering how biological sex impacts immune responses and COVID-19 outcomes. Nat Rev Immunol 20:442–447.

Song E et al. (2021a) Neuroinvasion of SARS-CoV-2 in human and mouse brain. J Exp Med 218:e20202135.

Song E et al. (2021b) Neuroinvasion of SARS-CoV-2 in human and mouse brain. J Exp Med 218:e20202135.

Soriano JB, Murthy S, Marshall JC, Relan P, Diaz JV, Condition WCCDWG on P-C-19 (2022) A clinical case definition of post-COVID-19 condition by a Delphi consensus. Lancet Infect Dis 22:e102–e107.

Spudich S, Nath A (2022) Nervous system consequences of COVID-19. Science 375:267–269.

Sudre CH et al. (2021) Attributes and predictors of long COVID. Nat Med 27:626–631.

Sun S-H et al. (2020) A Mouse Model of SARS-CoV-2 Infection and Pathogenesis. Cell Host Microbe 28:124-133.e4.

Surana P, Tang S, McDougall M, Tong CYW, Menson E, Lim M (2011) Neurological complications of pandemic influenza A H1N1 2009 infection: European case series and review. Eur J Pediatr 170:1007–1015.

Sutarjono B (2018) Can We Better Understand How Zika Leads to Microcephaly? A Systematic Review of the Effects of the Zika Virus on Human Brain Organoids. J Infect Dis 219:734–745.

Takahashi T et al. (2020a) Sex differences in immune responses that underlie COVID-19 disease outcomes. Nature 588:315–320.

Takahashi T et al. (2020b) Sex differences in immune responses that underlie COVID-19 disease outcomes. Nature:1–6.

Thompson PM, Dutton RA, Hayashi KM, Toga AW, Lopez OL, Aizenstein HJ, Becker JT (2005) Thinning of the cerebral cortex visualized in HIV/AIDS reflects CD4+ T lymphocyte decline. Proc Natl Acad Sci 102:15647–15652.

Weatherhead JE, Miller VE, Garcia MN, Hasbun R, Salazar L, Dimachkie MM, Murray KO (2015) Long-Term Neurological Outcomes in West Nile Virus–Infected Patients: An Observational Study. Am J Trop Med Hyg 92:1006–1012.

Wehbe Z, Hammoud SH, Yassine HM, Fardoun M, El-Yazbi AF, Eid AH (2021) Molecular and Biological Mechanisms Underlying Gender Differences in COVID-19 Severity and Mortality. Front Immunol 12:659339.

Wiley CA, Chimelli L (2017) Human Zika and West Nile virus neurological infections: What is the difference? Neuropathology 37:393–397.

Wong KT, Robertson T, Ong BB, Chong JW, Yaiw KC, Wang LF, Ansford AJ, Tannenberg A (2009) Human Hendra virus infection causes acute and relapsing encephalitis. Neuropath Appl Neuro 35:296–305.

Wouk J, Rechenchoski DZ, Rodrigues BCD, Ribelato EV, Faccin-Galhardi LC (2021a) Viral infections and their relationship to neurological disorders. Arch Virol 166:733–753.

Wouk J, Rechenchoski DZ, Rodrigues BCD, Ribelato EV, Faccin-Galhardi LC (2021b) Viral infections and their relationship to neurological disorders. Arch Virol 166:733–753.

Yeung MW, Shing E, Nelder M, Sander B (2017) Epidemiologic and clinical parameters of West

Nile virus infections in humans: a scoping review. BMC Infect Dis 17:609.

Zell R (2018) Picornaviridae—the ever-growing virus family. Arch Virol 163:299–317.

Zhang L, Gao S, White Z, Dai Y, Malik AB, Rehman J (2022) Single-cell transcriptomic profiling of lung endothelial cells identifies dynamic inflammatory and regenerative subpopulations. JCI Insight 7.

Zhang Z, Zhu Z, Chen W, Cai Z, Xu B, Tan Z, Wu A, Ge X, Guo X, Tan Z, Xia Z, Zhu H, Jiang T, Peng Y (2019) Cell membrane proteins with high N-glycosylation, high expression and multiple interaction partners are preferred by mammalian viruses as receptors. Bioinformatics 35:723–728.

Zhou F, Yu T, Du R, Fan G, Liu Y, Liu Z, Xiang J, Wang Y, Song B, Gu X, Guan L, Wei Y, Li H, Wu X, Xu J, Tu S, Zhang Y, Chen H, Cao B (2020) Clinical course and risk factors for mortality of adult inpatients with COVID-19 in Wuhan, China: a retrospective cohort study. Lancet Lond Engl 395:1054–1062.

Figure Legends

Figure 1. *Workflow for studying sex-specific development in the brain.* Gene expression data for 67 virus receptors across 15 brain areas were extracted from the Kang dataset and z-scored. This data was used to plot lifespan trajectories and identify differential gene expression ages between the sexes. Lifespan trajectories were visualized by fitting LOESS curves for each sex. The trajectories were then clustered in different ways to identify sex-specific brain development.

Figure 2. *Lifespan trajectories for ACE2 in the female and male brain.* For each of the 15 brain areas, z-scored expression values of Angiotensin Converting Enzyme 2 (ACE2), a key receptor for the Coronaviridae family viruses are plotted against age on a logarithmic scale. The curves are fitted using locally estimated scatterplot smoothing (LOESS), and the shaded bands indicate the 95% confidence interval. The curves are coloured by sex, with pink for females and blue for males. (A1C: primary auditory cortex, AMY: amygdala, CBC: cerebellar cortex, DFC: dorsolateral prefrontal cortex, HIP: hippocampus, IPC: posterior inferior parietal cortex, ITC: inferior temporal cortex, M1C: primary motor cortex, MFC: medial prefrontal cortex, OFC: orbital prefrontal cortex, S1C: primary somatosensory (S1) cortex, STC: superior temporal cortex, V1C: primary visual cortex, VFC: Ventrolateral prefrontal cortex, MD: mediodorsal nucleus of the thalamus).

Figure 3. *Clustering of developmental trajectories across 67 viral receptor genes in the female and male brain.* A) Hierarchical clustering dendrogram using the ward.D2 algorithm for 2010 developmental trajectories - representing 67 viral receptor genes across 15 brain areas. 25 clusters were identified and labelled according to percent female dominance. B) Average

trajectories for each cluster identified from the dendrogram reflect the average pattern of molecular development across the lifespan for all viral families across all brain areas.

Figure 4. *Sex differences across gene/brain area trajectory clusters.* A) Sex bias indices for each cluster from hierarchical clustering of 2010 developmental trajectories. B) Local maxima labelled on the average trajectory curves of the top female-dominated and top two male-dominated clusters. C) Frequencies of local maxima by age for hierarchical clustering of 2010 lifespan trajectories.

Figure 5. *Venn Diagrams for the 25 clusters.* Clusters were determined using ward.d2 hierarchical clustering of the 2010 developmental trajectories. Venn diagrams were used to identify genes with similar lifespan trajectories in females and males. The clusters are ordered from most to least female-dominated.

Figure 6. *Cluster Composition: Brain Areas.* For each cluster determined by hierarchical clustering of 2010 lifespan trajectories, the percentage of trajectories specific to a particular brain area is shown. Colour progression from warm to cool corresponds to anatomical progression of brain areas studied from most rostral (OFC) to most caudal (CBC). Clusters are ordered by percent female dominance.

Figure 7. *Cluster Composition: Viral Families.* For each cluster determined by hierarchical clustering of 2010 lifespan trajectories, the distribution of viral families is shown for each of the 15 brain areas studied. Clusters are ordered by percent female dominance.

Figure 8. *Average curves for clusters within viral families.* Developmental trajectories for each viral family were clustered independently using the ward.D2 algorithm for hierarchical clustering. Average curves reflect representative patterns of gene expression through time for each cluster. For each viral family, clusters are ordered by percent female dominance.

Figure 9. *Venn diagrams from clusters within viral families.* Clusters were obtained using the ward.D2 algorithm for hierarchical clustering of each viral family independently, and are ordered by percent female dominance for each viral family.

Figure 10. *Within-family cluster composition: brain areas.* Distribution of brain areas for each cluster obtained from hierarchical clustering of each viral family independently. Colour progression from warm to cool corresponds to anatomical progression of brain areas studied from most rostral (OFC) to most caudal (CBC).

Figure 11. *Within viral family cluster composition: viral species.* Within each family, and for each cluster, the proportions of viral species that compose a cluster is shown. Clusters were determined independently for each viral family using the ward.D2 algorithm for hierarchical clustering.

Figure 12. *Sex bias and sexual dimorphism across viral families.* (A-J) Sex bias index results for each cluster within a viral family. Clusters were obtained independently for each family using the ward.D2 algorithm for hierarchical clustering. (K) Sexual dimorphism score for each viral family. The colour of the bar indicates dimorphism, and the saturation of purple indicates the degree of dimorphism.

Figure 13. *Differential Expression Sliding Window Analysis (DESWAN) for the 15 brain areas.* The DESWAN heatmaps have a row for each virus gene, and a column for each reference age. The rows are ordered by a surrounding dendrogram, to group similar patterns of gene expression together. Higher expression in females is shown in pink, and higher expression in males is shown in green.

Figure 14. *Differential Expression Sliding Window Analysis (DESWAN) for DFC, A1C and HIP.* Differential Expression Sliding Window Analysis (DE-SWAN) plots showing sex-specific

patterns of gene expression in A) Dorsolateral Prefrontal Cortex (DFC), B) Primary Auditory Cortex (A1C), C) Hippocampus (HIP). Blue asterisks indicate receptors for WNV; Orange asterisks indicate receptors for EV and RABV; Grey asterisks indicate receptors for SARS-CoV-2 and IAV.

Figure 15. *Visualizing high-dimensional developmental trajectories in 15 brain areas.* Density preserving t-SNE plots to visualize and compare the development of virus receptors in the 15 brain areas for females and males. A) colour-code by the 4 clusters, B) colour-coded by age (light is young and darker red is old). C) colour-coded by sex and cortical vs subcortical shows distinct sex-specific cortical clusters

Supplementary Figures

Supplementary Figure 1. *Lifespan trajectories.* Locally Estimated Scatterplot Smoothing (Loess) curves plotted for all 67 genes across all 15 brain areas studied. Z-scored expression values are plotted against age on a logarithmic scale. Shaded bands indicate the 95% confidence interval, and curves are coloured by sex.

Supplementary Figure 2. *Clustering profile for each viral family.* A) Dendrogram for hierarchical clustering of developmental trajectories for genes associated with each viral family. Clustering was performed for each viral family independently. B) Average curves for each cluster for each viral family, ordered by decreasing percent female dominance. C) Venn diagrams representing the percent female dominance for each cluster. D) Pie charts showing percent representation of brain areas within each cluster. Colour progression from warm to cool reflects anatomical progression of brain areas studied from rostral(OFC) to caudal (CBC). E) Pie

charts showing which viral species compose each cluster. F) Heatmaps showing the proportions of trajectories for each virus receptor gene within each cluster, ordered by correlating percent female dominance. Navy indicates absence of a trajectory for a gene, and shades of yellow show varying proportions of trajectories.

Supplementary Figure 3. *Average trajectories for each brain area.* Using the ward.d2 algorithm for hierarchical clustering, developmental trajectories were clustered for each brain area independently. Clusters are ordered by decreasing percent female dominance.

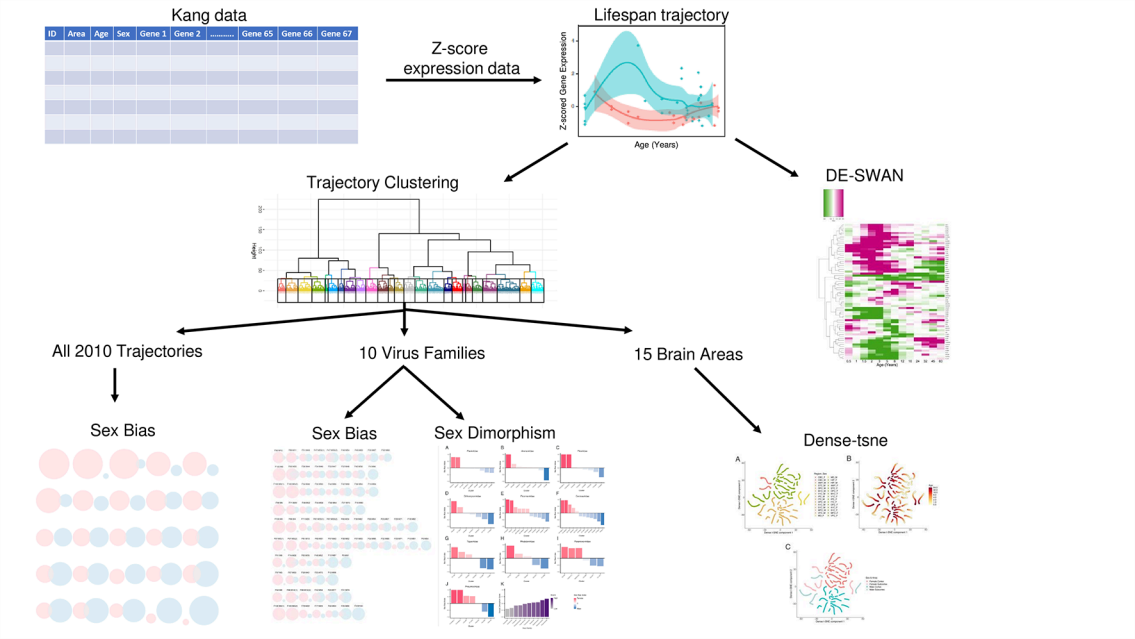
Kang data
ID
Area
Age
Sex
Gene 1
Gene 2
.....
Gene 65
Gene 66
Gene 67
Z-score
expression data
Lifespan trajectory
Z-scored Gene Expression
Age (Years)
Trajectory Clustering
DE-SWAN
All 2010 Trajectories
10 Virus Families
15 Brain Areas
Sex Bias
Sex Bias
Sex Dimorphism
Dense-tsne

Coronaviridae, . Human coronavirus NL63 , SARS coronavirus , Severe acute respiratory syndrome coronavirus 2 **ACE2** , (Receptor)

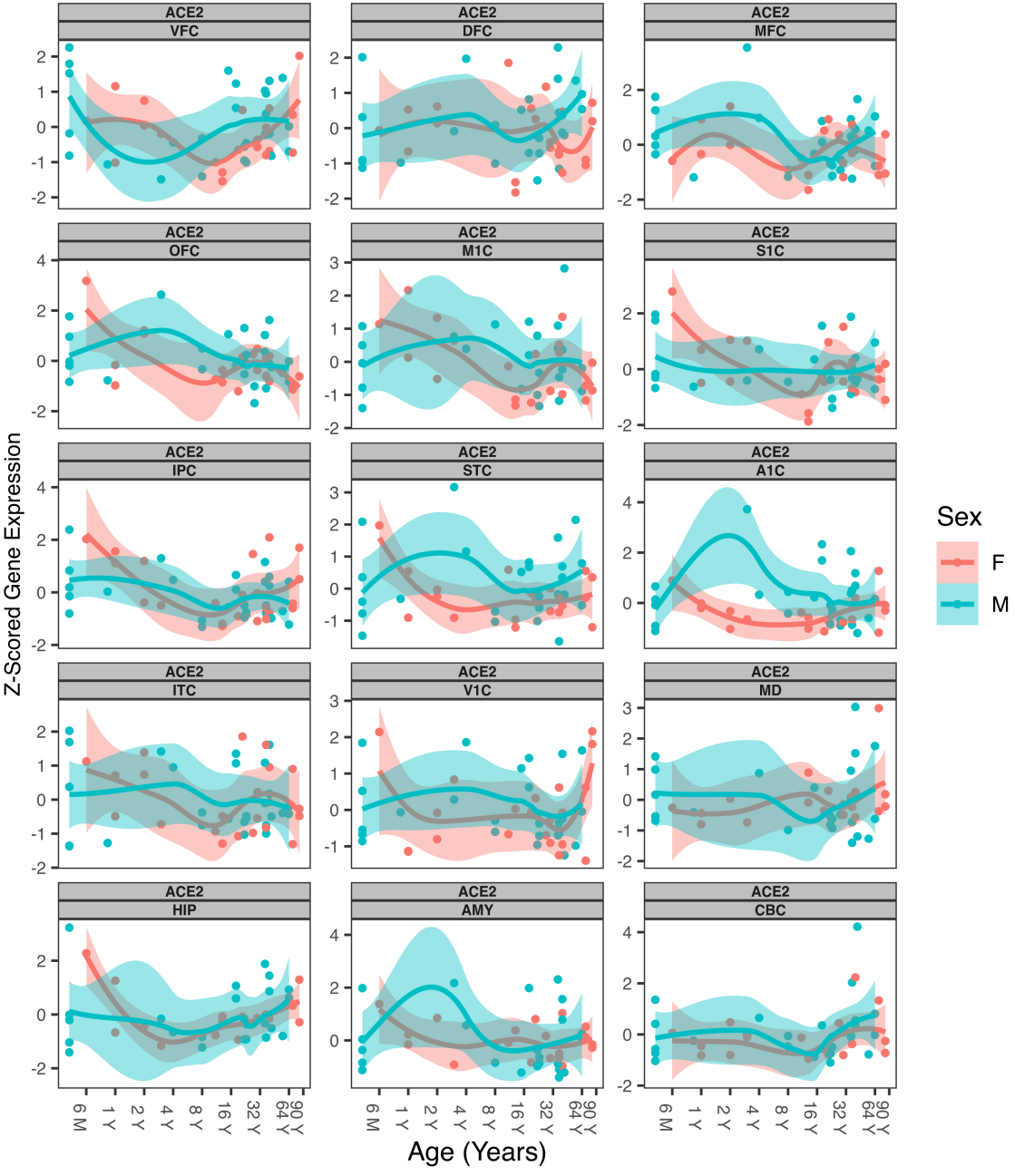

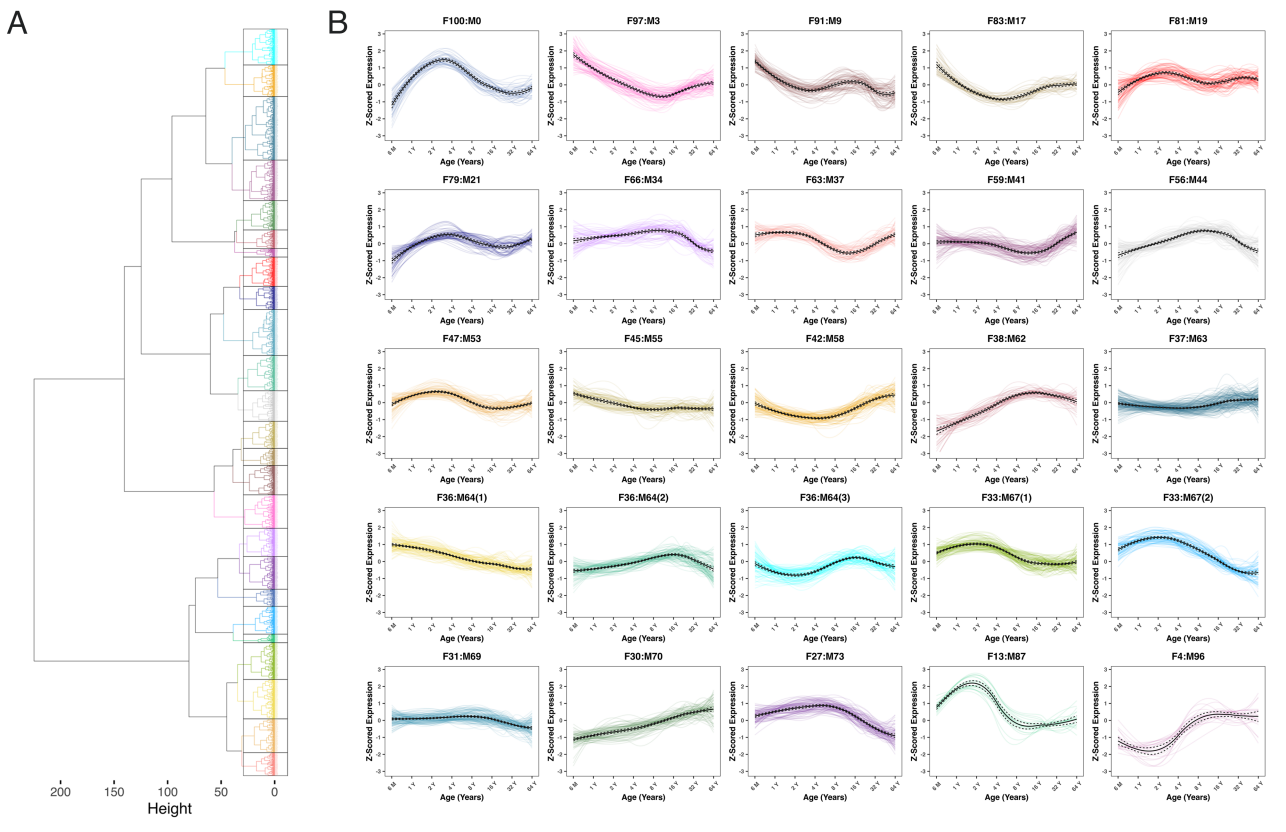
A
200
150
100
50
0
Height
B
F100:M0
F97:M3
F91:M9
F83:M17
F81:M19
F79:M21
F66:M34
F63:M37
F59:M41
F56:M44
F47:M53
F45:M55
F42:M58
F38:M62
F37:M63
F36:M64(1)
F36:M64(2)
F36:M64(3)
F33:M67(1)
F33:M67(2)
F31:M69
F30:M70
F27:M73
F13:M87
F4:M96
Z-Scored Expression
Age (Years)

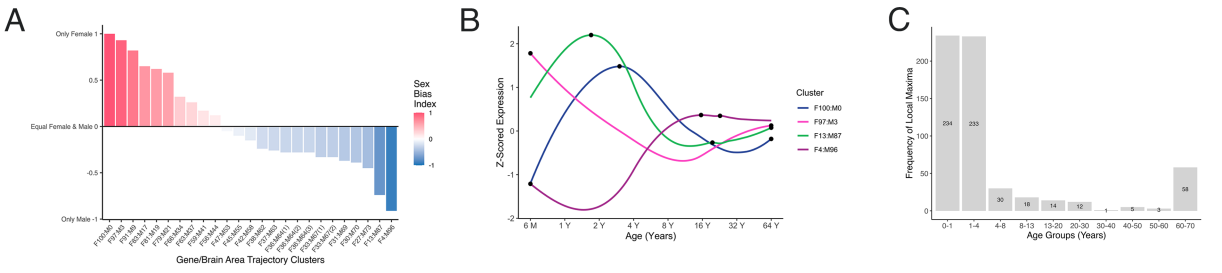
A
Only Female 1
0.5
Equal Female & Male 0
-0.5
Only Male -1
Sex Bias Index
1
0
-1
F100:M0
F97:M3
F81:M9
F83:M17
F81:M19
F79:M21
F68:M34
F63:M37
F59:M41
F56:M44
F47:M53
F45:M55
F42:M58
F39:M62
F37:M63
F36:M64(1)
F36:M64(2)
F36:M64(3)
F33:M67(1)
F33:M67(2)
F31:M69
F30:M70
F27:M73
F13:M87
F4:M96
Gene/Brain Area Trajectory Clusters
B
Z-Scored Expression
2
1
0
-1
-2
6 M
1 Y
2 Y
4 Y
8 Y
16 Y
32 Y
64 Y
Age (Years)
Cluster
F100:M0
F97:M3
F13:M87
F4:M96
C
Frequency of Local Maxima
200
150
100
50
0
234
233
30
18
14
12
1
5
3
58
0-1
1-4
4-8
8-13
13-20
20-30
30-40
40-50
50-60
60-70
Age Groups (Years)

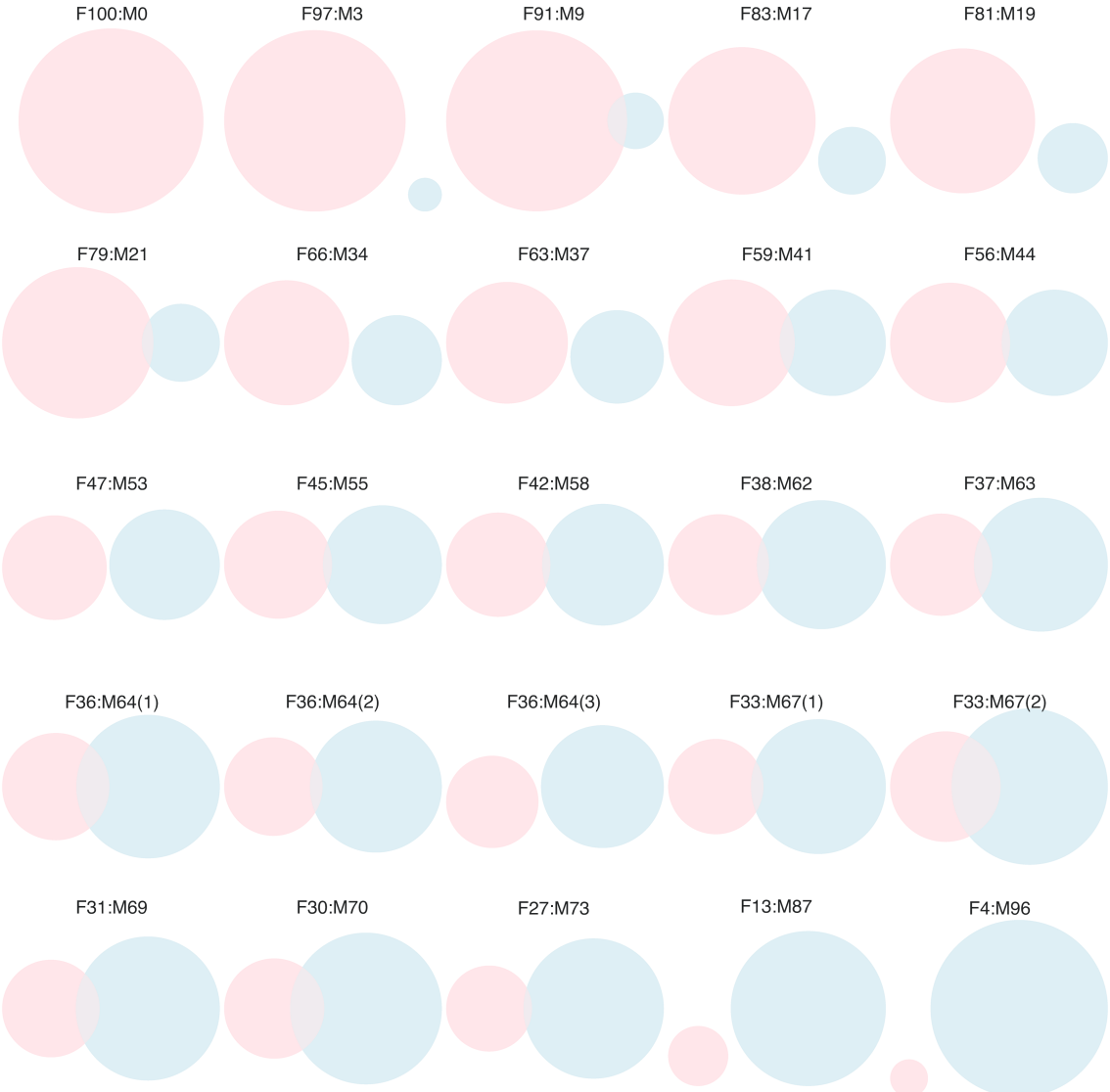
F100:M0
F97:M3
F91:M9
F83:M17
F81:M19
F79:M21
F66:M34
F63:M37
F59:M41
F56:M44
F47:M53
F45:M55
F42:M58
F38:M62
F37:M63
F36:M64(1)
F36:M64(2)
F36:M64(3)
F33:M67(1)
F33:M67(2)
F31:M69
F30:M70
F27:M73
F13:M87
F4:M96

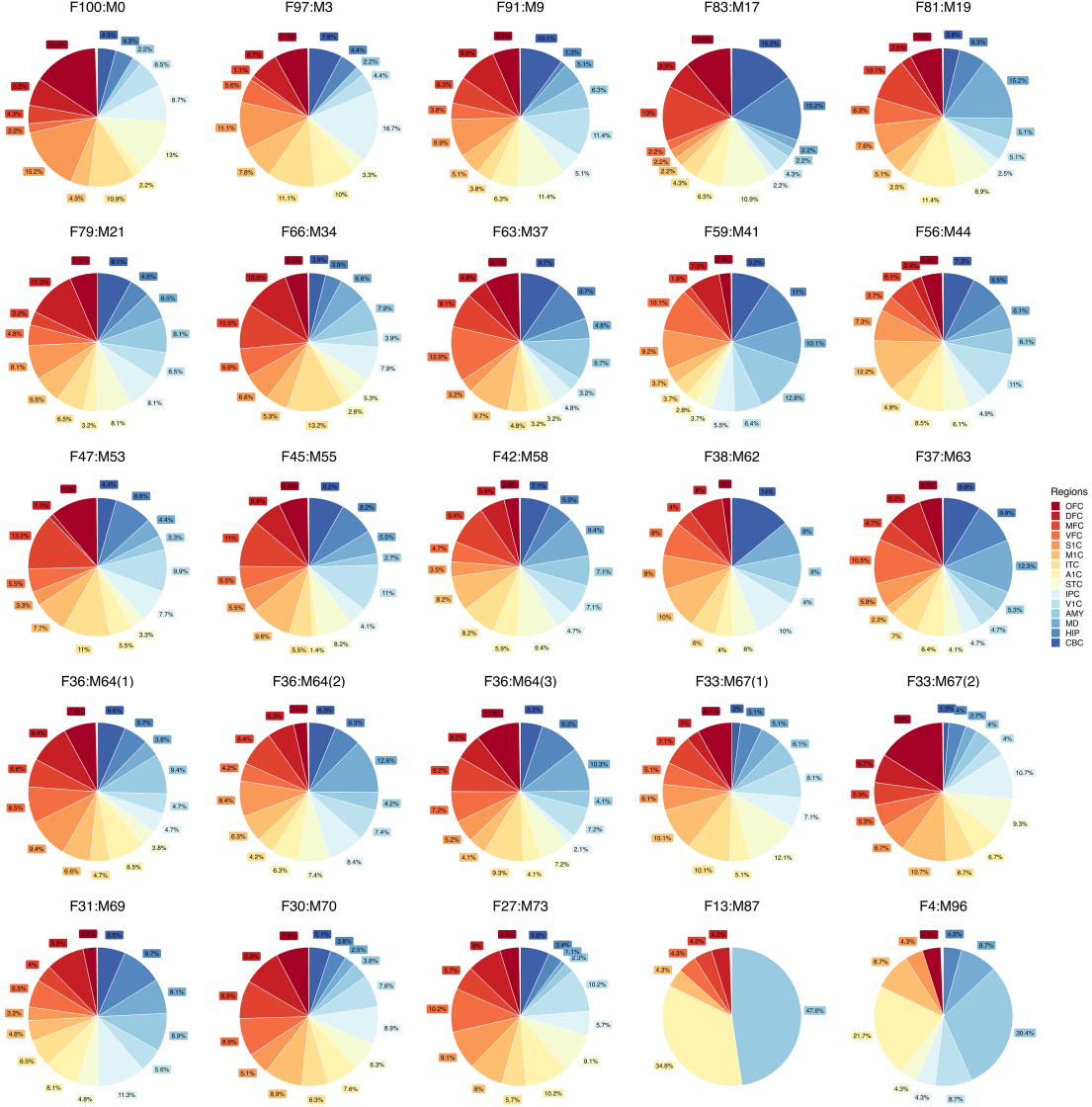
F100:M0
F97:M3
F91:M9
F83:M17
F81:M19
F79:M21
F66:M34
F63:M37
F59:M41
F56:M44
F47:M53
F45:M55
F42:M58
F38:M62
F37:M63
F36:M64(1)
F36:M64(2)
F36:M64(3)
F33:M67(1)
F33:M67(2)
F31:M69
F30:M70
F27:M73
F13:M87
F4:M96
Regions
OFC
DFC
MFC
VFC
S1C
M1C
ITC
A1C
STC
IPC
V1C
AMY
MD
HIP
CBC

F100:M0
F97:M3
F91:M9
F83:M17
F81:M19
F79:M21
F66:M34
F63:M37
F59:M41
F56:M44
F47:M53
F45:M55
F42:M58
F38:M62
F37:M63
F36:M64(1)
F36:M64(2)
F36:M64(3)
F33:M67(1)
F33:M67(2)
F31:M69
F30:M70
F27:M73
F13:M87
F4:M96
Families
Arenaviridae
Coronaviridae
Filoviridae
Flaviviridae
Orthomyxoviridae
Paramyxoviridae
Picornaviridae
Pneumoviridae
Rhabdoviridae
Togaviridae

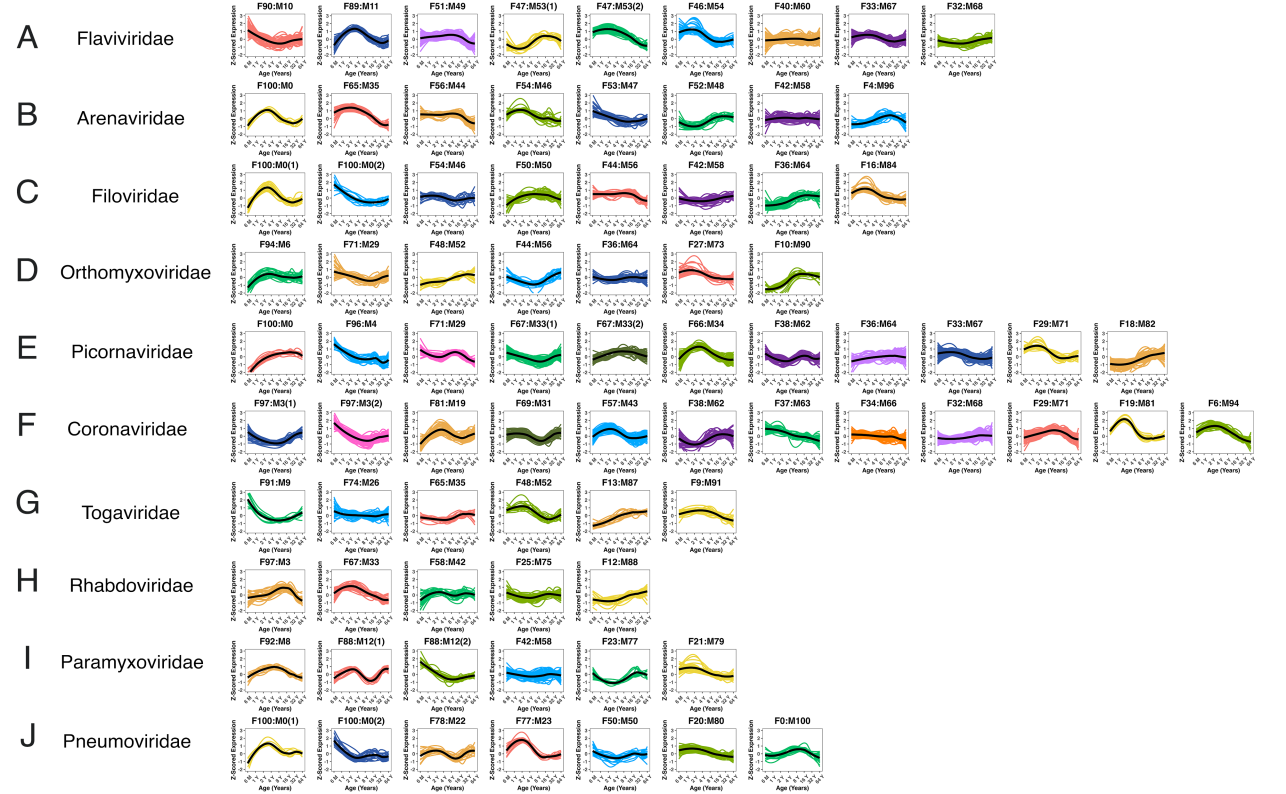
A
Flaviviridae
F90:M10
F89:M11
F51:M49
F47:M53(1)
F47:M53(2)
F46:M54
F40:M60
F33:M67
F32:M68
B
Arenaviridae
F100:M0
F65:M35
F56:M44
F54:M46
F53:M47
F52:M48
F42:M58
F4:M96
C
Filoviridae
F100:M0(1)
F100:M0(2)
F54:M46
F50:M50
F44:M56
F42:M58
F36:M64
F16:M84
D
Orthomyxoviridae
F94:M6
F71:M29
F48:M52
F44:M56
F36:M64
F27:M73
F10:M90
E
Picornaviridae
F100:M0
F96:M4
F71:M29
F67:M33(1)
F67:M33(2)
F66:M34
F38:M62
F36:M64
F33:M67
F29:M71
F18:M82
F
Coronaviridae
F97:M3(1)
F97:M3(2)
F81:M19
F69:M31
F57:M43
F38:M62
F37:M63
F34:M66
F32:M68
F29:M71
F19:M81
F6:M94
G
Togaviridae
F91:M9
F74:M26
F65:M35
F48:M52
F13:M87
F9:M91
H
Rhabdoviridae
F97:M3
F67:M33
F58:M42
F25:M75
F12:M88
I
Paramyxoviridae
F92:M8
F88:M12(1)
F88:M12(2)
F42:M58
F23:M77
F21:M79
J
Pneumoviridae
F100:M0(1)
F100:M0(2)
F78:M22
F77:M23
F50:M50
F20:M80
F0:M100
Z-Scored Expression
Age (Years)

A
Flaviviridae
F90:M10
F89:M11
F51:M49
F47:M53(1)
F47:M53(2)
F46:M54
F40:M60
F33:M67
F32:M68
B
Arenaviridae
F100:M0
F65:M35
F56:M44
F54:M46
F53:M47
F52:M48
F42:M58
F4:M96
C
Filoviridae
F100:M0(1)
F100:M0(2)
F54:M46
F50:M50
F44:M56
F42:M58
F36:M64
F16:M84
D
Orthomyxoviridae
F96:M6
F71:M29
F48:M52
F44:M56
F36:M64
F27:M73
F10:M90
E
Picornaviridae
F100:M0
F96:M4
F71:M29
F67:M33(1)
F67:M33(2)
F66:M34
F38:M62
F36:M64
F33:M67
F29:M71
F18:M82
F
Coronaviridae
F97:M3(1)
F97:M3(2)
F81:M19
F69:M31
F57:M43
F38:M62
F37:M63
F34:M66
F32:M68
F29:M71
F19:M81
F6:M94
G
Togaviridae
F91:M9
F74:M26
F65:M35
F48:M52
F13:M87
F9:M91
H
Rhabdoviridae
F97:M3
F67:M33
F58:M42
F25:M75
F12:M88
I
Paramyxoviridae
F92:M8
F88:M12(1)
F88:M12(2)
F42:M58
F23:M77
F21:M79
J
Pneumoviridae
F100:M0(1)
F100:M0(2)
F78:M22
F77:M23
F50:M50
F20:M80
F0:M100

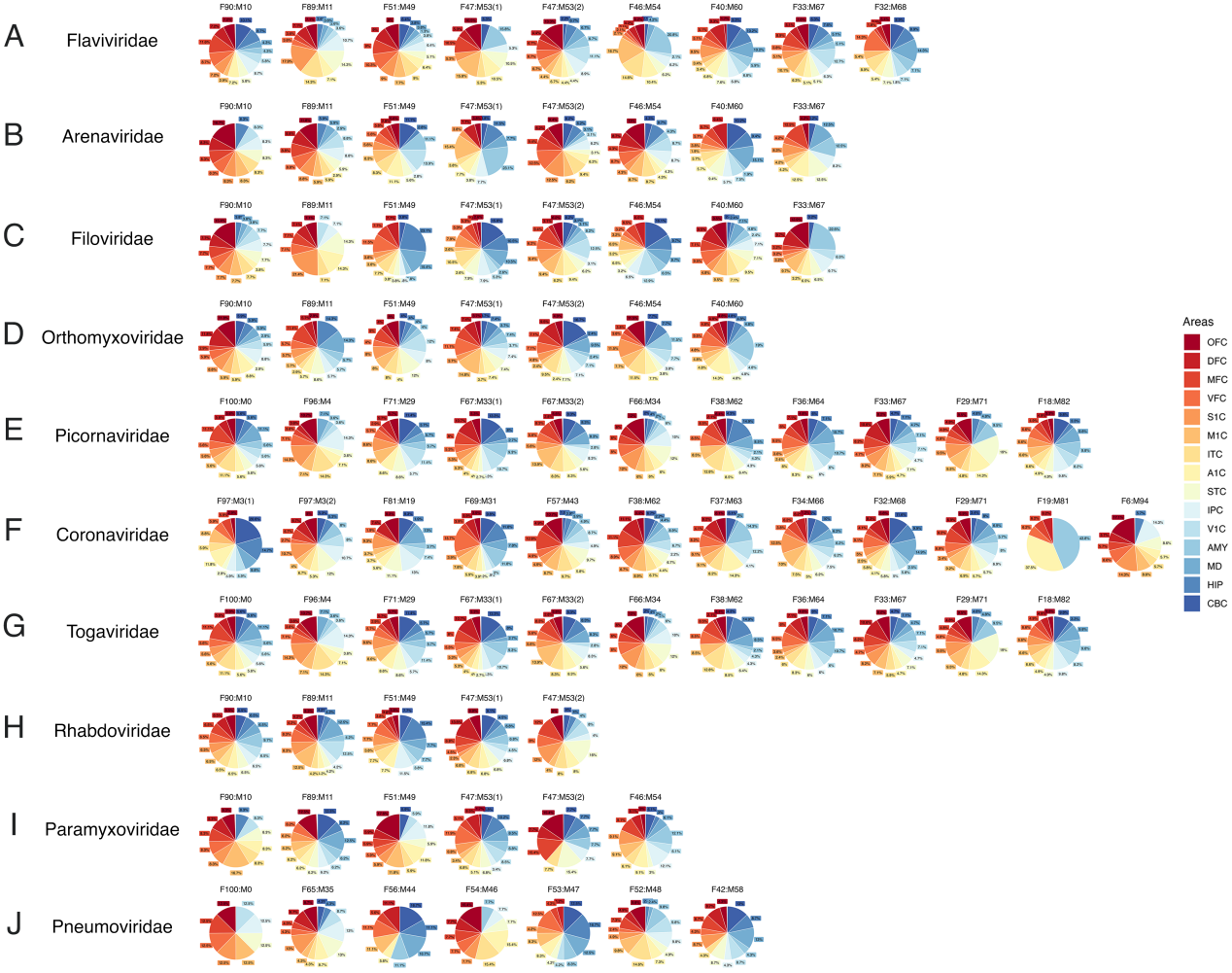
A
Flaviviridae
F90:M10
F89:M11
F51:M49
F47:M53(1)
F47:M53(2)
F46:M54
F40:M60
F33:M67
F32:M68
B
Arenaviridae
F90:M10
F89:M11
F51:M49
F47:M53(1)
F47:M53(2)
F46:M54
F40:M60
F33:M67
C
Filoviridae
F90:M10
F89:M11
F51:M49
F47:M53(1)
F47:M53(2)
F46:M54
F40:M60
F33:M67
D
Orthomyxoviridae
F90:M10
F89:M11
F51:M49
F47:M53(1)
F47:M53(2)
F46:M54
F40:M60
E
Picornaviridae
F100:M0
F96:M4
F71:M29
F67:M33(1)
F67:M33(2)
F66:M34
F38:M62
F36:M64
F33:M67
F29:M71
F18:M82
F
Coronaviridae
F97:M3(1)
F97:M3(2)
F81:M19
F69:M31
F57:M43
F38:M62
F37:M63
F34:M66
F32:M68
F29:M71
F19:M81
F6:M94
G
Togaviridae
F100:M0
F96:M4
F71:M29
F67:M33(1)
F67:M33(2)
F66:M34
F38:M62
F36:M64
F33:M67
F29:M71
F18:M82
H
Rhabdoviridae
F90:M10
F89:M11
F51:M49
F47:M53(1)
F47:M53(2)
I
Paramyxoviridae
F90:M10
F89:M11
F51:M49
F47:M53(1)
F47:M53(2)
F46:M54
J
Pneumoviridae
F100:M0
F65:M35
F56:M44
F54:M46
F53:M47
F52:M48
F42:M58
Areas
OFC
DFC
MFC
VFC
S1C
M1C
ITC
A1C
STC
IPC
V1C
AMY
MD
HIP
CBC

A
Flaviviridae
F90:M10
F89:M11
F51:M49
F47:M53(1)
F47:M53(2)
F46:M54
F40:M60
F33:M67
F32:M68
Virus Species
Dengue virus
Hepacivirus C
Japanese encephalitis virus
West Nile virus
Zika virus
B
Arenaviridae
F100:M0
F65:M35
F56:M44
F54:M46
F53:M47
F52:M48
F42:M58
F4:M96
Virus Species
Argentinian mammarenavirus
Guanarito mammarenavirus
Lassa mammarenavirus
Latino mammarenavirus
Lymphocytic choriomeningitis mammarenavirus
Machupo mammarenavirus
Oliveros mammarenavirus
C
Filoviridae
F100:M0(1)
F100:M0(2)
F54:M46
F50:M50
F44:M56
F42:M58
F36:M64
F16:M84
Virus Species
Ebola virus
Marburg marburgvirus
D
Orthomyxoviridae
F94:M6
F71:M29
F48:M52
F44:M56
F36:M64
F27:M73
F10:M90
Virus Species
Influenza A virus
E
Picornaviridae
F100:M0
F96:M4
F71:M29
F67:M33(1)
F67:M33(2)
F66:M34
F38:M62
F36:M64
F33:M67
F29:M71
F18:M82
Virus Species
Coxsackievirus A
Coxsackievirus B
Echovirus E
Enxephalomyocarditis virus
Enterovirus A
Enterovirus B
Enterovirus C
Enterovirus D
Hepatovirus
Human enterovirus
Human parechovirus
Human rhinovirus A
Rhinovirus B
Rhinovirus C
F
Coronaviridae
F97:M3(1)
F97:M3(2)
F81:M19
F69:M31
F57:M43
F38:M62
F37:M63
F34:M66
F32:M68
F29:M71
F19:M81
F6:M94
Virus Species
Human coronavirus 229E
Human coronavirus NL63
Middle East respiratory syndrome-related coronavirus
SARS coronavirus
Severe acute respiratory syndrome coronavirus 2
G
Togaviridae
F91:M9
F74:M26
F65:M35
F48:M52
F13:M87
F9:M91
Virus Species
Chikungunya virus
Rubella virus
Sindbis virus
Venezuelan equine encephalitis virus
H
Rhabdoviridae
F97:M3
F67:M33
F58:M42
F25:M75
F12:M88
Virus Species
Rabies lyssavirus
Vesicular stomatitis virus
I
Paramyxoviridae
F92:M8
F88:M12(1)
F88:M12(2)
F42:M58
F23:M77
F21:M79
Virus Species
Hendra henipavirus
Measles morbillivirus
Nipah henipavirus
J
Pneumoviridae
F100:M0(1)
F100:M0(2)
F78:M22
F77:M23
F50:M50
F20:M80
F0:M100
Virus Species
Human metapneumovirus
Respiratory syncytial virus

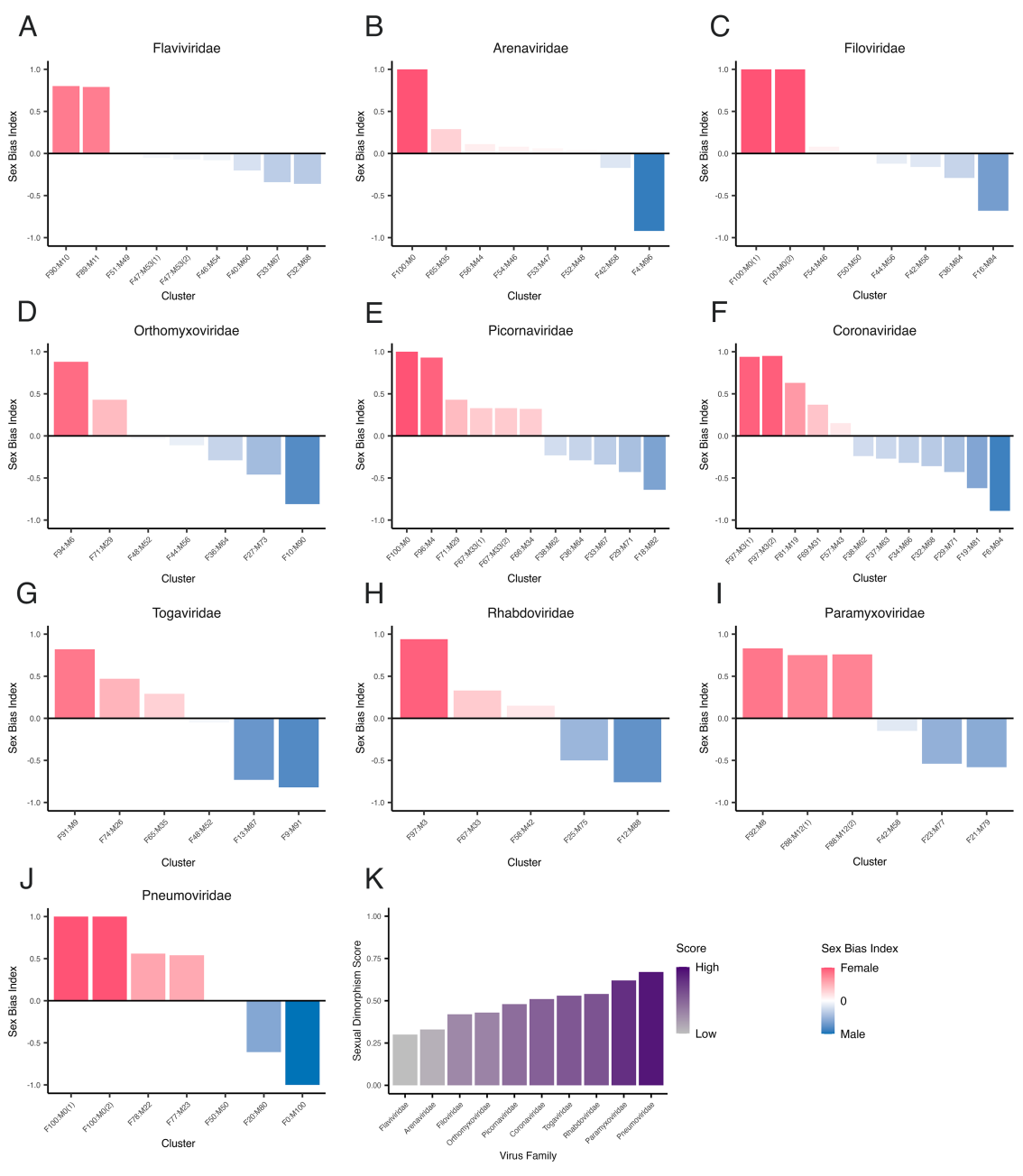
A
Flaviviridae
Sex Bias Index
1.0
0.5
0.0
-0.5
-1.0
F90:M10
F89:M11
F51:M49
F47:M53(1)
F47:M53(2)
F46:M54
F40:M60
F33:M67
F32:M68
Cluster
B
Arenaviridae
Sex Bias Index
F100:M0
F65:M35
F56:M44
F54:M46
F53:M47
F52:M48
F42:M58
F4:M96
Cluster
C
Filoviridae
Sex Bias Index
F100:M0(1)
F100:M0(2)
F54:M46
F50:M50
F44:M56
F42:M58
F36:M64
F16:M84
Cluster
D
Orthomyxoviridae
Sex Bias Index
F94:M6
F71:M29
F48:M52
F44:M56
F39:M64
F27:M73
F10:M90
Cluster
E
Picornaviridae
Sex Bias Index
F100:M0
F96:M4
F71:M29
F67:M33(1)
F67:M33(2)
F66:M34
F38:M62
F36:M64
F33:M67
F29:M71
F18:M82
Cluster
F
Coronaviridae
Sex Bias Index
F97:M3(1)
F97:M3(2)
F91:M19
F89:M31
F57:M43
F38:M62
F37:M63
F34:M66
F32:M68
F29:M71
F19:M81
F6:M94
Cluster
G
Togaviridae
Sex Bias Index
F91:M9
F74:M26
F65:M35
F48:M52
F13:M87
F9:M91
Cluster
H
Rhabdoviridae
Sex Bias Index
F97:M3
F67:M33
F58:M42
F25:M75
F12:M88
Cluster
I
Paramyxoviridae
Sex Bias Index
F92:M8
F88:M12(1)
F88:M12(2)
F42:M58
F23:M77
F21:M79
Cluster
J
Pneumoviridae
Sex Bias Index
F100:M0(1)
F100:M0(2)
F78:M22
F77:M23
F50:M50
F20:M80
F0:M100
Cluster
K
Sexual Dimorphism Score
1.00
0.75
0.50
0.25
0.00
Flaviviridae
Arenaviridae
Filoviridae
Orthomyxoviridae
Picornaviridae
Coronaviridae
Togaviridae
Rhabdoviridae
Paramyxoviridae
Pneumoviridae
Virus Family
Score
High
Low
Sex Bias Index
Female
0
Male

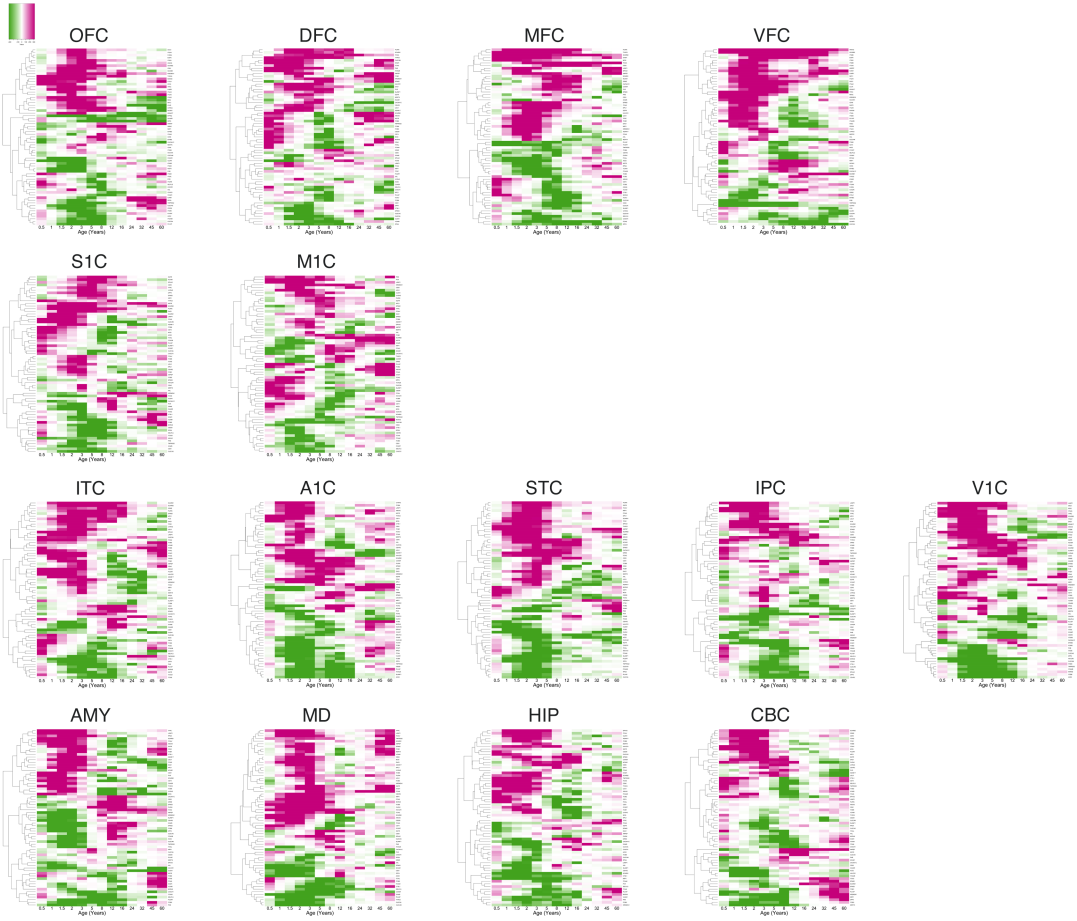
OFC
DFC
MFC
VFC
S1C
M1C
ITC
A1C
STC
IPC
V1C
AMY
MD
HIP
CBC
Age (Years)

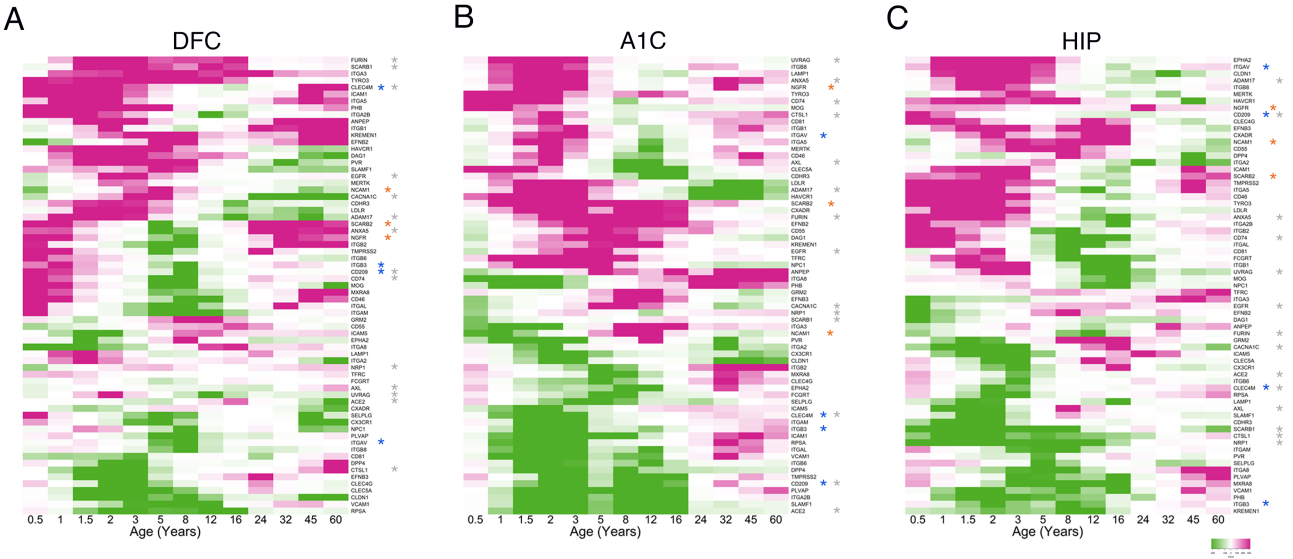
A
DFC
FURIN
SCARB1
ITGA3
TYRO3
CLEC4M
ICAM1
ITGA5
PHB
ITGA2B
ANPEP
ITGB1
KREMEN1
ENB2
HAVCR1
DAG1
PVR
SLAMF1
EGFR
MERTK
NCAM1
CACNA1C
CDHR3
LDLR
ADAM17
SCARB2
ANXA5
NGFR
ITGB2
TMPRSS2
ITGB8
ITGB3
CD209
CD74
MOG
MXRA8
CD46
ITGAL
ITGAM
GRM2
CD55
ICAM5
EPHA2
ITGA8
LAMP1
ITGA2
NRP1
TFRC
FCGRT
AXL
UVRAG
ACE2
CX3CR1
SELPLG
CXCR1
CLDN1
PLVAP
ITGAV
ITGB6
CD81
DPP4
CTSL1
EFNB3
CLEC4G
CLEC5A
CLDN1
VCAM1
RPSA
0.5 1 1.5 2 3 5 8 12 16 24 32 45 60
Age (Years)
B
A1C
UVRAG
ITGB8
LAMP1
ANXA5
NGFR
TYRO3
CD74
MOG
CTSL1
CD81
ITGB1
ITGA5
PHB
MERTK
CD46
AXL
CLEC5A
CDHR3
LDLR
ADAM17
HAVCR1
SCARB2
CX3CR
FURIN
EFNB2
CD55
DAG1
KREMEN1
EGFR
TFRC
NPC1
ANPEP
ITGA8
PHB
GRM2
EFNB3
CACNA1C
NRP1
SCARB1
ITGA3
NCAM1
PVR
ITGA2
CX3CR1
CLDN1
ITGB2
MXRA8
CLEC4G
EPHA2
FCGRT
SELPLG
ICAM5
CLEC4M
ITGAM
ITGB3
ITGA6
RPSA
ITGAL
VCAM1
ITGB6
DPP4
TMPRSS2
CD209
PLVAP
ITGA2B
SLAMF1
ACE2
0.5 1 1.5 2 3 5 8 12 16 24 32 45 60
Age (Years)
C
HIP
EPHA2
ITGAV
CLDN1
ADAM17
ITGB8
MERTK
HAVCR1
NGFR
CD209
CLEC4G
EFNB3
CX3CR
ICAM1
FCGRT
DPP4
ITGA2
ICAM1
SCARB2
TMPRSS2
ITGA5
CD46
TYRO3
LDLR
ANXA5
ITGA2B
ITGB2
CD74
ITGAL
CD81
FCGRT
ITGB1
UVRAG
MOG
NPC1
TFRC
ITGA3
EGFR
EFNB2
DAG1
ANPEP
FURIN
GRM2
CACNA1C
ICAM5
CLEC5A
CX3CR1
ACE2
ITGB6
CLEC4M
RPSA
LAMP1
AXL
SLAMF1
CDHR3
SCARB1
CTSL1
NRP1
ITGAM
PVR
SELPLG
ITGA8
PLVAP
MXRA8
VCAM1
PHB
ITGB3
KREMEN1
0.5 1 1.5 2 3 5 8 12 16 24 32 45 60
Age (Years)

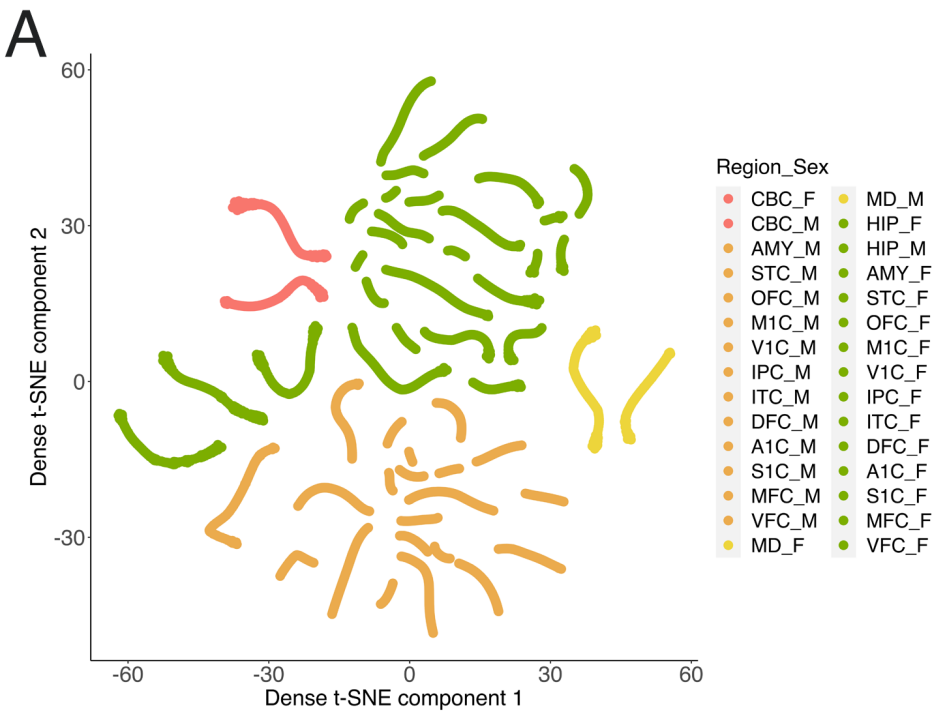
A
Dense t-SNE component 2
Dense t-SNE component 1
60
30
0
-30
-60
-30
0
30
60
Region_Sex
CBC_F
CBC_M
AMY_M
STC_M
OFC_M
M1C_M
V1C_M
IPC_M
ITC_M
DFC_M
A1C_M
S1C_M
MFC_M
VFC_M
MD_F
MD_M
HIP_F
HIP_M
AMY_F
STC_F
OFC_F
M1C_F
V1C_F
IPC_F
ITC_F
DFC_F
A1C_F
S1C_F
MFC_F
VFC_F

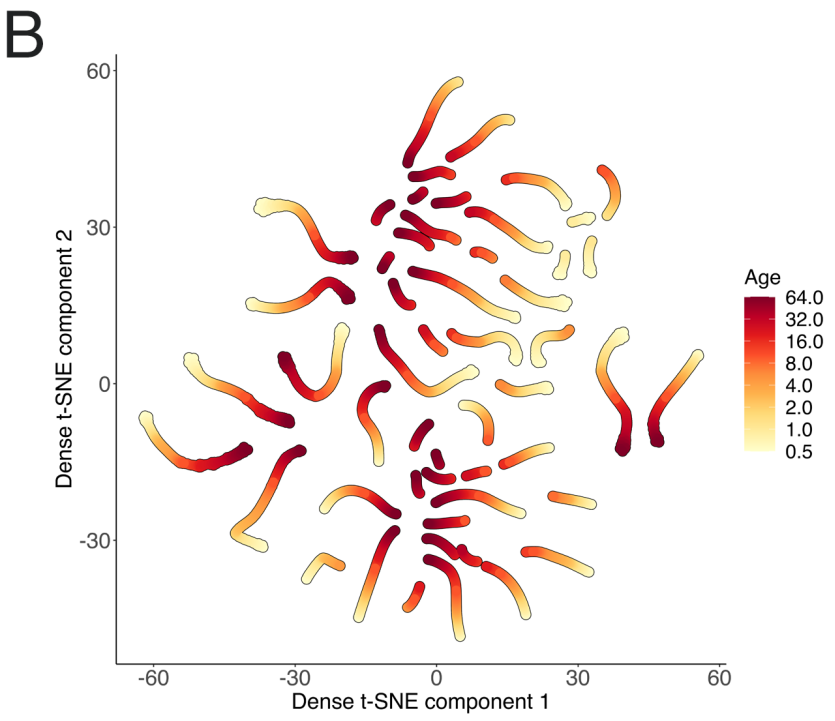
B
Dense t-SNE component 2
Dense t-SNE component 1
60
30
0
-30
-60
-30
0
30
60
Age
64.0
32.0
16.0
8.0
4.0
2.0
1.0
0.5

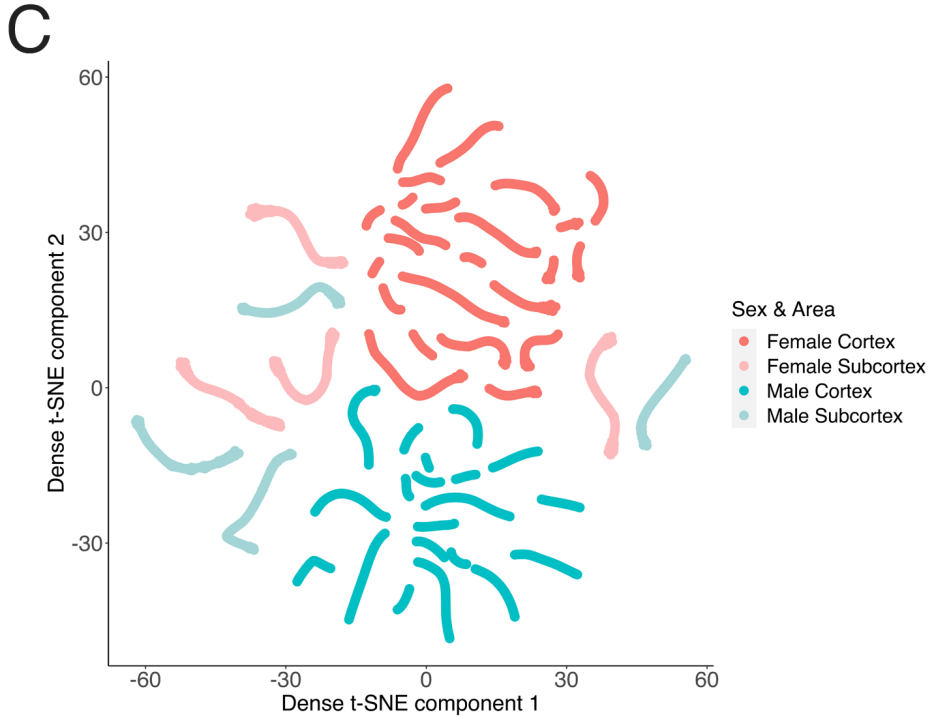
C
Dense t-SNE component 2
Dense t-SNE component 1
60
30
0
-30
-60
-30
0
30
60
Sex & Area
Female Cortex
Female Subcortex
Male Cortex
Male Subcortex